

## Pharmacophore-Based Design of Phenyl-[hydroxycyclohexyl] Cycloalkyl-Carboxamide Mitofusin Activators with Improved Neuronal Activity

Xiawei Dang, Sidney B. Williams, Sriram Devanathan, Antonietta Franco, Lijun Fu, Peter R. Bernstein, Daniel Walters, and Gerald W. Dorn, II\*

Cite This: <https://doi.org/10.1021/acs.jmedchem.1c00163>

Read Online

ACCESS |



Metrics &amp; More

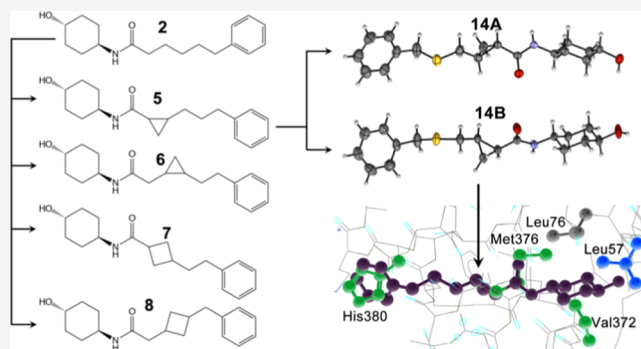


Article Recommendations



Supporting Information

**ABSTRACT:** Mitochondrial fragmentation from defective fusion or unopposed fission contributes to many neurodegenerative diseases. Small molecule mitofusin activators reverse mitochondrial fragmentation *in vitro*, promising a novel therapeutic approach. The first-in-class mitofusin activator, **2**, has a short plasma  $t_{1/2}$  and limited neurological system bioavailability, conferring “burst activation”. Here, pharmacophore-based rational redesign generated analogues of **2** incorporating cycloalkyl linker groups. A cyclopropyl-containing linker, **5**, improved plasma and brain  $t_{1/2}$ , increased nervous system bioavailability, and prolonged neuron pharmacodynamic effects. Functional and single-crystal X-ray diffraction studies of stereoisomeric analogues of **5** containing sulfur as a “heavy atom”, **14A** and **14B**, showed that **5** biological activity resides in the *trans*-R/R configuration, **5B**. Structural analysis revealed stereoselective interactions of **5** associated with its mimicry of MFN2 Val372, Met376, and His380 side chains. Modification of murine ALS phenotypes *in vitro* and *in vivo* supports advancement of **5B** for neurological conditions that may benefit from sustained mitofusin activation.



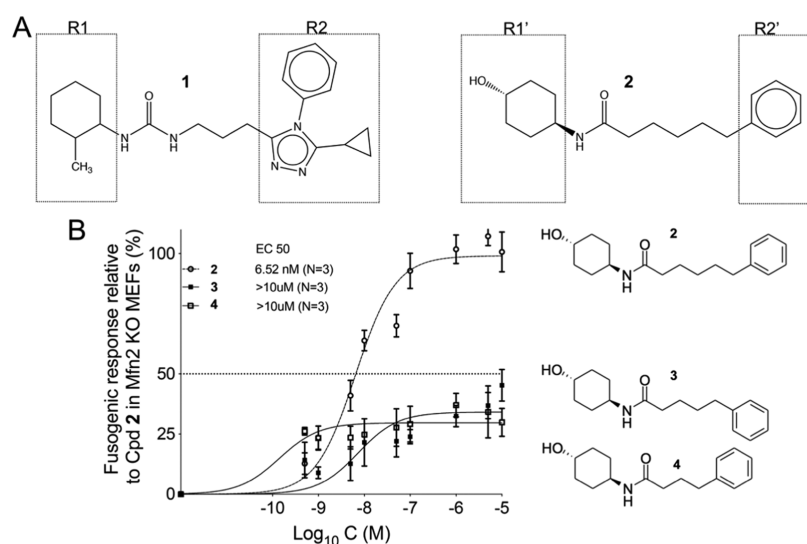
## INTRODUCTION

Mitochondrial fragmentation caused by an imbalance between mitochondrial fusion and fission is a common cause of, and contributor to, neurodegenerative diseases.<sup>1,2</sup> Mitochondrial fusion is initiated by outer mitochondrial membrane-embedded mitofusin (MFN) proteins whose extra-organellar domains extend across the cytosolic space to interact with counterparts on the neighboring mitochondria, physically linking organelles *via* MFN–MFN dimers/oligomers.<sup>3</sup> Mitofusins subsequently induce the outer mitochondrial membrane fusion through a process requiring catalytic GTPase activity.<sup>4–6</sup> Multiple mitofusin 2 (MFN2) mutations, most frequently located within the MFN2 GTPase domain, are implicated in a rare untreatable childhood sensory-motor neuropathy, Charcot–Marie–Tooth (CMT) disease type 2A.<sup>7,8</sup> Defects in mitofusin function or expression are also described in other neurodegenerative conditions, including experimental amyotrophic lateral sclerosis<sup>9</sup> and clinical Huntington’s disease.<sup>10</sup> For these reasons, mitofusins are attractive drug targets.<sup>11</sup>

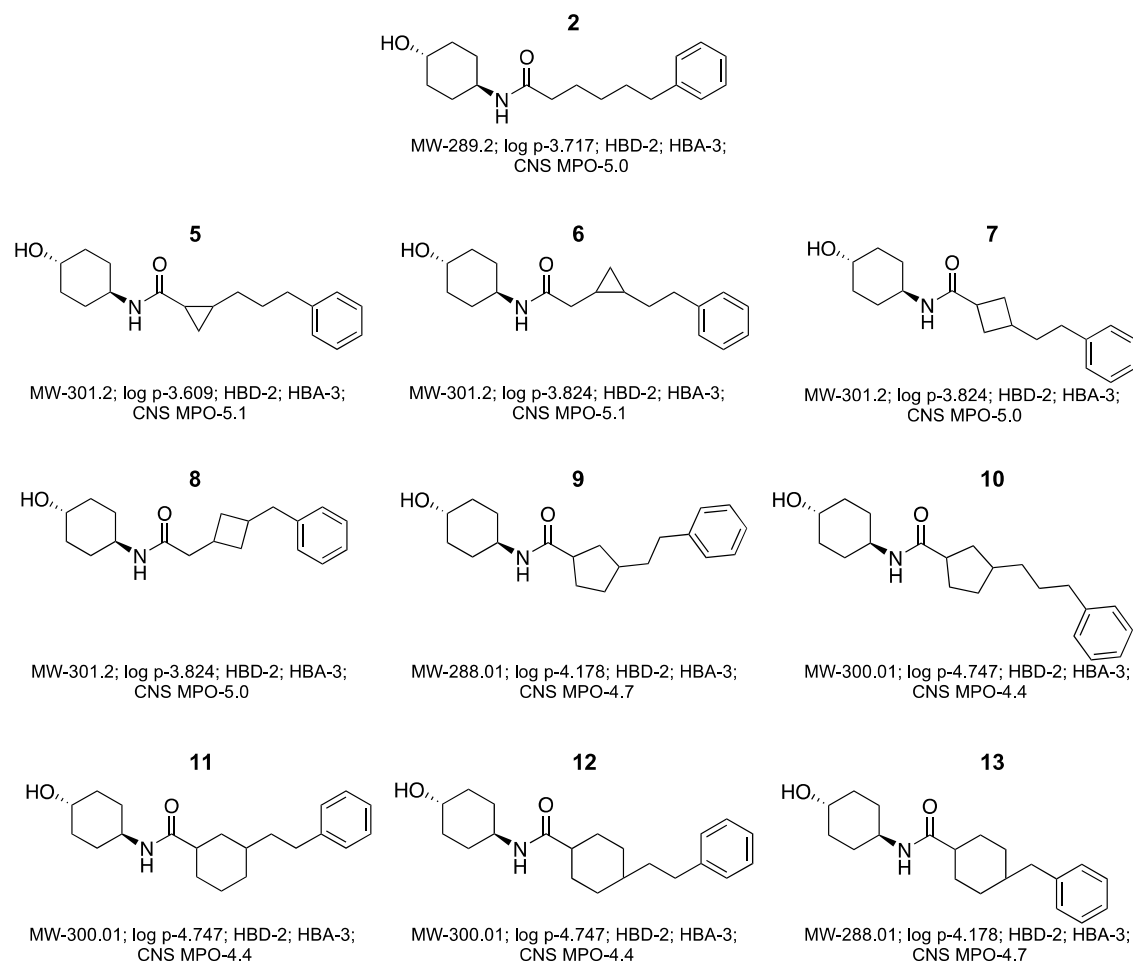
Developing a pharmaceutically acceptable activator of mitofusins to enhance mitochondrial fusion was challenging. The antirheumatic drug leflunomide was identified as a transcriptional enhancer of mitofusin mRNA expression, but effective concentrations are high (10–50  $\mu$ M).<sup>12</sup> A putative small molecule mitofusin activator, 4-chloro-2-(1-(2-(2,4,6-

trichlorophenyl) hydrazineylidene) ethyl)phenol, was detected by high-throughput screening for fusogenic compounds, but with an  $EC_{50}$  of 4–5  $\mu$ M, it also has limited utility except as a research tool.<sup>13</sup> Franco et al. designed an 18 amino acid cell-permeant mitofusin-activating peptide modified from hMFN2 amino acids 367–384 that could be introduced into cells using the amino terminal TAT<sub>47–57</sub> conjugation.<sup>14</sup> This peptide activates mitofusins by competing for and disrupting intramolecular peptide–peptide bonds enforcing the closed (inactive) mitofusin protein conformation and has greater potency for mitofusin stimulation than the above compounds ( $EC_{50} \sim 0.3 \mu$ M). However, as peptides, their therapeutic utility in clinical diseases seems limited. Thus, Rocha et al.<sup>15</sup> developed small triazolurea-containing molecules, like **1**, that potently induce mitochondrial fusion ( $EC_{50} \sim 5$  nM) by mimicking function-critical amino acids of the Franco activator

Received: January 28, 2021



**Figure 1.** Structures of triazolurea (1) and phenylhexanamide (2) mitofusin activators. (A) Both classes of mitofusin activator share a substituted cyclohexyl (R1, R1') linked to an aromatic moiety (R2, R2') by a six- or seven-membered alkyl linker. (B) Dose–response relationships for mitochondrial elongation (measured as the increase in the mitochondrial aspect ratio) of 2 and its analogues having one (3) or two (4) fewer carbons in the alkyl linker.

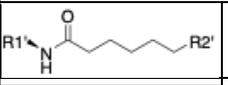
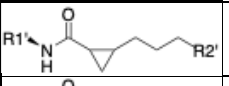
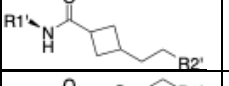
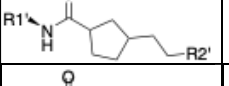
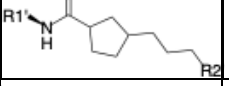
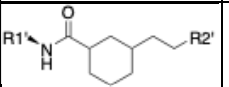
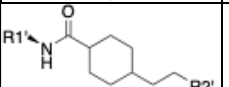
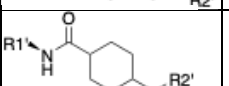


**Figure 2.** Designs for variants of 2 having cycloalkyl linkers. Calculated Lipinski's rule values and central nervous system multiparameter optimization desirability (MPO) factors are shown below. MW, molecular weight; log *p*, octanol–water partition coefficient; HBD, number of hydrogen bond donors; and HBA, number of hydrogen bond acceptors.

peptide. Unfortunately, mitofusin activators with this chemical structure proved incompatible with *in vivo* use.<sup>16</sup>

Phenylhexanamide mitofusin activators possessing drug-like properties were recently described.<sup>16</sup> The lead compound of

Table 1. Functional and Pharmacokinetic Properties of Cycloalkyl Linker 2 Variants<sup>a</sup>

	EC50 (nM)	Plasma Protein Binding (% Bound)		Liver Microsomes (t <sub>1/2</sub> , min)		PAMPA (Pe, 10 <sup>-6</sup> cm/s)	
		human	mouse	human	mouse		
	2	5.8	91	96.3	>145	92.4	26
	5	5.1	94.4	95.5	>145	114.1	58
	6	5.6	89.1	93.1	>145	76.7	39
	7	11	97.2	94.3	>145	105.5	61
	8	85	95.3	93.5	>145	124.9	37
	9	7	97.73	95.97	>145	35.1	114
	10	15.3	99.25	98.8	120.2	43.2	154
	11	4.8	97.77	4.03	69.2	20.5	126
	12	7.4	99.59	98.86	>145	74.4	133
	13	44.6	92.05	94.43	>145	49.3	88.8

<sup>a</sup>Linker modifications of **2** are shown on the left-hand side; functional and PK characteristics are shown on the right-hand side. R1' is cyclohexanol and R2' is phenyl as in Figure 1. EC<sub>50</sub> 95% confidence limits are shown in Figure S1.

this chemical series (**2**) demonstrated *in vivo* engagement of neuronal mitochondria after intravenous administration; its daily intramuscular administration reversed neuromuscular degeneration in a mouse model of CMT2A.<sup>17</sup> However, this compound has a short half-life in mouse plasma (*t*<sub>1/2</sub> 1.1 h) and brain (*t*<sub>1/2</sub> 1.06 h), properties most suitable for “burst activation” of mitofusins.<sup>17</sup> We posited that mitofusin activators having a more prolonged presence in the central nervous system could have greater therapeutic utility in other neurodegenerative conditions.

Here, we extended mitofusin activator design by employing the previously described pharmacophore-based strategy.<sup>16</sup> We considered that structurally more rigid and metabolically stable compounds resulting from introduction of cycloalkyl modifications into the hexanamide linker<sup>18–21</sup> might have a greater engagement of neuronal mitochondria. In particular, introduction of cyclopropyl rings into different compounds has increased potency, selectivity, oral bioavailability, metabolic and chemical stability, or neurological system exposure. Relevant to our pharmacophore-based design strategy, cyclopropyl rings have been employed to restrict the conformation of the serotonin and norepinephrine reuptake inhibitor Z-milnacipran and the monoamine oxidase inhibitor tranylcypamine.<sup>21</sup> Here, a preclinical lead compound having a linker cyclopropyl group, **5**, exhibited potent stereospecific mitofusin activation and longer plasma and brain *t*<sub>1/2</sub> than **2**. Single-

crystal X-ray crystallography of **5** sulfide analogues [**14A** and **14B**] revealed that the (*trans-R,R*) enantiomer uniquely conferred mitofusin agonist activity. The crystal structure moiety distances and hydrogen-bonding characteristics mimicked those of function-critical amino acid side chains within the precursor mitofusin agonist peptide, consistent with the pharmacophore model. *In vitro* and *in vivo* proof-of-concept studies with **5B** in murine amyotrophic lateral sclerosis (ALS) support its clinical development for neurodegenerative diseases linked to mitochondrial dysfunction.

## RESULTS AND DISCUSSION

**Rational Redesign of Mitofusin Activators.** Prototype triazolurea (**1**) and phenylhexanamide (**2**) mitofusin agonists share the general structure of a substituted cyclohexyl group (R1) connected to an aromatic moiety (R2) by urea- or carboxamide-containing alkyl linkers (Figure 1A). The linker promotes optimal spacing between R1 and R2, which according to the pharmacophore model,<sup>15</sup> respectively, mimic human MFN2 His380 and Met376/Val372. The linker can be a source of conformational plasticity, but the published pharmacophore model and reported structure–activity relationships<sup>15,16</sup> suggest that mitofusin activators can be modified to retain biological activity if the R1–R2 separation distance is conserved. Indeed, deletion of one (**3**) or two (**4**) carbons from the **2** linker largely abrogated mitofusin activation

measured as the ability to promote mitochondrial fusion (increased aspect ratio: length/width) (Figure 1B). Accordingly, we posited that the introduction of small cycloalkyl linker groups that do not alter the R1–R2 distance could both stabilize the molecule and enhance passive membrane permeability reported to correlate with blood–brain barrier penetration.<sup>16</sup> Structures and characteristics of parent **2** and nine cycloalkyl linker analogues are shown in Figure 2.

**In Vitro Characterization of Mitofusin Activators with Cycloalkyl Linkers.** To gauge how pharmacophore modeling conformed to reality, mitofusin activation by **5**–**13** was compared using the mitochondrial elongation fusogenicity assay in MFN2-deficient cells.<sup>14–16</sup> Because the *trans*-cyclohexanol stereoisomer of parent **2** was biologically active whereas the corresponding *cis*-analogue was not,<sup>16</sup> **5**–**13** were each synthesized as *trans*-stereoisomers at this position. The cyclopropyl analogues, **5** and **6**, were potent mitofusin activators having EC<sub>50</sub> values for mitochondrial elongation similar to parent **2**, *i.e.*, ~5–6 nM (Table 1). There was no clear benefit to increasing the size of linker cycloalkyl groups, which increased PAMPA Pe but also increased instability in the mouse liver microsomal assay (Table 1 and Figure S1).

**In Vivo Pharmacokinetic Properties of 5.** Among the newly synthesized and characterized cycloalkyl linker analogues of **2**, *in vitro* characteristics of **5** appeared pharmaceutically most favorable. Therefore, *in vivo* PK studies of **5** were undertaken in mice, the species in which all previous PK studies of mitofusin activators have been performed.<sup>16</sup> Plasma **5** levels were measured at increasing times after administration of single 10 mg/kg intravenous (IV) doses. Compared to published values for **2**,<sup>16</sup> **5** had ~50% longer plasma elimination *t*<sub>1/2</sub> and proportionally greater tissue distribution (V<sub>dss</sub>) values, with correspondingly reduced peak plasma and AUC levels (Table 2).

Table 2. *In Vivo* Pharmacokinetic Properties of **5**<sup>a</sup>

	<b>5</b>	<b>2</b>
dose (mg/kg)	10	10
C <sub>0</sub> (ng/mL)	32 111	50 600
<i>t</i> <sub>1/2</sub> (h)	1.64	1.1
AUC <sub>0–last</sub> (ng·h/mL)	9178	11 495
V <sub>dss</sub> (L/kg)	0.6	0.347

<sup>a</sup>IV administration in mice, 10 mg/kg; values for **2** are from ref 16.

**Fusogenicity and Mitofusin Interactions of 5 Are Stereoisomer-Specific.** Because only the *trans*-cyclohexanol stereoisomer of **2** has biological activity,<sup>16</sup> **5**–**13** were

synthesized as *trans*-isomers at the cyclohexanol group. However, the linker cyclopropyl group in **5** creates additional chiral centers to either side, with four possible stereoisomers (Figure 3, left). Chiral separation of **5** by supercritical fluid chromatography (SFC-H) identified only two isomers, designated -A and -B for the faster and slower eluting forms, respectively (Figure 3, right). Proton NMR of synthetic intermediate **5C** revealed a coupling constant of ~19 Hz for the olefin proton at 6.75 ppm, indicating a *trans*-olefin geometry (Figure S2). In agreement with expectations based on the known reaction mechanism, the product of the Corey–Chaykovsky reaction leading to **5** (synthetic Scheme 2) contained only two isomers: *trans*-*R,R* and *S,S* (Figure 3).

Mitofusin-stimulating activities of **5A** and **5B** were compared by assaying their effects on mitochondrial elongation and polarization status in Mfn1-null (*i.e.*, expressing Mfn2 alone) or Mfn2-null (*i.e.*, expressing Mfn1 only) murine embryonic fibroblasts (Figure 4). The prototype triazole mitofusin activator, **1**, was assayed in parallel as a historical comparator. There were little effects produced by **5A** (1 μM, 48 h) on either outcome. By comparison, **5B** was equipotent with **1** in cells expressing either Mfn1 or Mfn2. Thus, **5B** is a potent mitofusin activator.

We tested **5A** and **5B** interactions with the MFN2 protein using a previously described Förster resonance energy-transfer (FRET) assay that measures MFN2 conformational changes provoked by mitofusin activators.<sup>15–17</sup> Please note that FRET assays were performed on isolated mitochondria, whereas assessments of mitochondrial elongation were performed in intact cells. A high compound concentration (1 μM) was employed to test whether inactivity of enantiomer **5A** to promote mitochondrial elongation in cells corresponded with FRET inactivity for *in vitro* target engagement. As shown in Figure 5, **5B** had the same effect on MFN2 conformation previously described for mitofusin activators **1**<sup>15</sup> and **2**<sup>16</sup> *i.e.*, it decreased the FRET signal, reflecting separation of the N-terminal mCerulean and C-terminal mVenus fluorophores after unfolding of the protein into its active conformation. By comparison, **5A** did not decrease the FRET signal. Thus, **5A** did not conformationally activate MFN2.

**X-ray Diffraction Reveals Enantiomeric Structures of 5A and 5B.** Although **5A** and **5B** were determined to be the *trans*-cyclopropyl stereoisomers (*vide supra*), it was not possible to assign *R,R* vs *S,S* structures to the stereoisomers. Thus, we synthesized heavier sulfide analogues of **5A** and **5B** for X-ray diffraction studies, designated **14A** and **14B**, respectively (Figure 6A). Like their respective parents, **14B** potently stimulated mitochondrial elongation in Mfn2-null

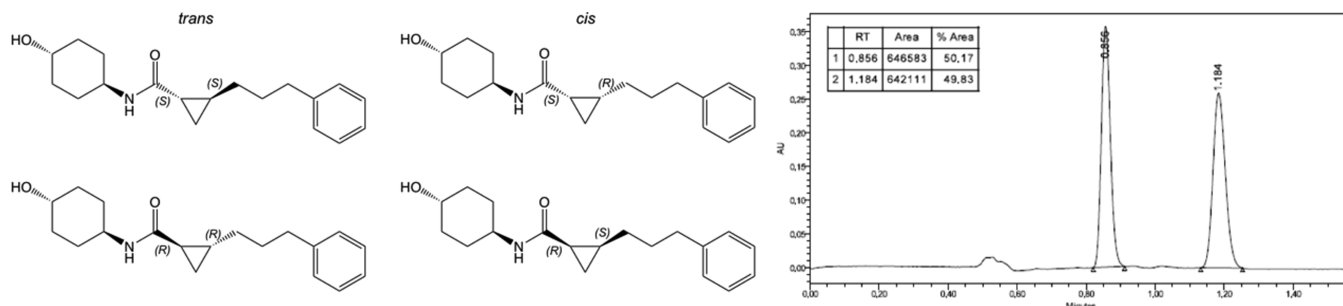
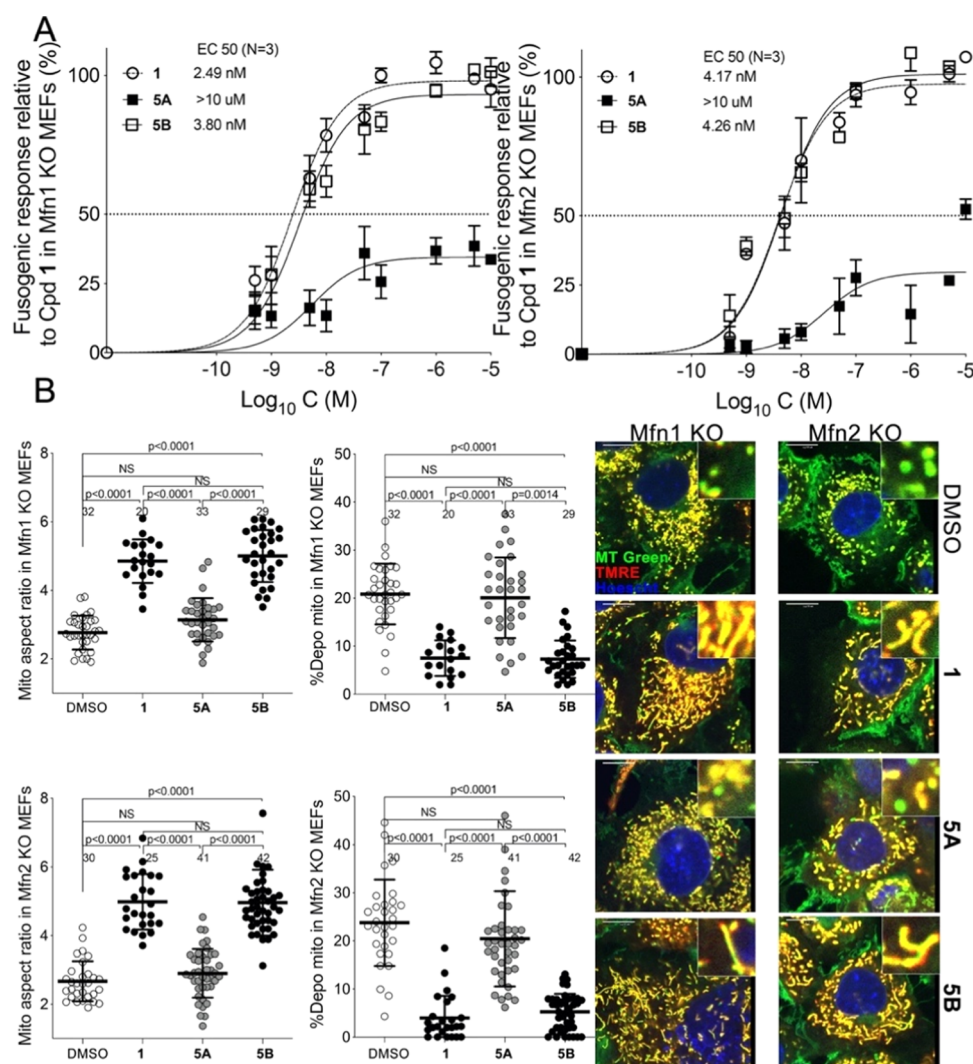


Figure 3. Synthesis of **5** results in a ~50:50 mixture of **5** *trans*-stereoisomers. Left, structures of the four possible **5** stereoisomers. Right, chiral separation identifies two forms, shown to be *trans*-based on <sup>1</sup>H NMR of synthetic intermediate **5C** (Figure S2).



**Figure 4.** Mitochondrial elongation and polarization-enhancing activities of 5 enantiomers. (A) Dose–response curves for 5A and 5B to increase the mitochondrial aspect ratio (length/width) in cultured fibroblasts lacking Mfn1 (left, 5A: EC<sub>50</sub> > 10 μM, 5B: EC<sub>50</sub> = 3.80 nM; 95% confidence limits, 2.70–5.28 nM) or Mfn2 (right, 5A: EC<sub>50</sub> > 10 μM, 5B: EC<sub>50</sub> = 4.26 nM; 95% confidence limits, 2.99–6.04 nM). Parallel studies with prototype mitofusin activator 1 are shown for comparison. (B) Group data (left) and representative live cell confocal micrographs (right) from Mfn1 and Mfn2-null cells showing mitochondrial elongation (increase in aspect ratio) and reversal of depolarization with a 1 μM test compound added for 48 h. Enlarged mitochondria are shown in the insets. Mitochondria staining yellow are highly polarized, *i.e.*, healthy; green staining mitochondria are depolarized and dysfunctional.

fibroblasts, whereas 14A had poor biological activity (Figure 6B).

The X-ray powder diffraction patterns and small rodlike crystal morphologies under polarized light microscopy of 14A and 14B were similar (Figure S3). Crystals used for single-crystal X-ray diffraction (SCXRD) for 14A were obtained by slow evaporation in acetonitrile (Figure S4A) and for 14B by slow evaporation in ethyl acetate (Figure S4B). As anticipated from studies of synthetic intermediates of 5 (see Figure 3), the resulting crystal structures showed that the two compounds are enantiomers, with 14B displaying {*R,R*} chirality.

Crystalline structures of 14A and 14B displayed no disorder. The asymmetric unit cells contained one molecule of the compound with no solvent molecules present (Figure 7A). Indeed, crystals with identical morphology readily formed out of multiple solvent systems (Table S1). The packing diagram (Figure 7B) and hydrogen-bonding network between 14B molecules connecting in two directions (Figure 7C) further support the absence of solvent molecules. Thus, 14B molecules

form a pseudo-polymeric structure connected by the amide moieties near the center of the molecule. The carbonyl oxygen (O10) forms strong hydrogen-bonding interactions with the hydrogens of adjacent molecules' amide nitrogen (N8).

The hydrogen-bonding distance measured by the donor–acceptor distance is 2.887 Å. This contact deviates only slightly from the idealized hydrogen geometry as measured by linearity including the idealized H8A across the O10–N8 angle (171.31°). A second hydrogen-bonding interaction dimerizes these pseudo-polymeric structures across the terminal alcohol (O1) with a donor–acceptor distance of 2.745 Å, reflecting an even stronger interaction. This is likely the consequence of every involved alcohol being both donor and acceptor, polarizing each oxygen involved. The resulting zig-zag formation and O–O–O angle of 130.72° are conducive to a trigonal planar-type interaction.

Bonds within the 14B cyclopropyl moiety are slightly uneven: the longest interaction is the backbone C11–C13 bond (1.515 Å), while the adjoining bonds are asymmetrical,

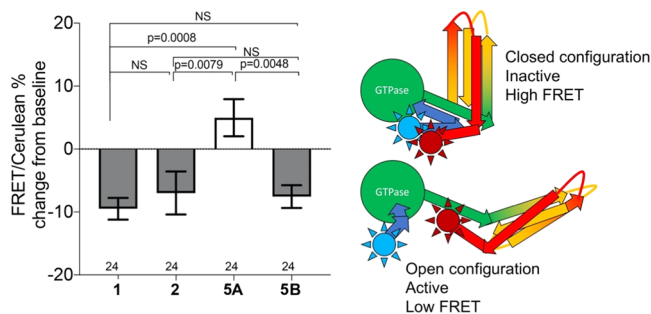


**Figure 5.** MFN2 altering activity of **5** is stereoisomer-specific. Results of FRET studies comparing MFN2 conformation altering activities of prototype mitofusin activators **1** and **2** with **5** stereoisomers (all compounds added to a final concentration of 1  $\mu$ M as in Figure 4B; assays were performed after 4 h). Decreased FRET signal reflects MFN2 unfolding as depicted to the right. Blue sun indicates the position of the amino terminal mCerulean; red sun is C-terminal mVenus. Means  $\pm$  standard error of the mean (SEM) of six separate studies with four to six replicates each.

with a longer bond on the carbon  $\alpha$  to the electropositive amide carbon (C11–C12, 1.513 Å) and a shorter bond on the carbon  $\beta$  to the electron-donating sulfur (C13–C12, 1.484 Å). The molecule as a whole, if measured across the two hydrogen atoms idealized upon the two farthest atoms, is 18.415 Å in length. Simulation of the mimicked environment for **14A** and **14B** within hMFN2 is depicted in Figure 8. Positions of human MFN2 amino acids His380, Met376, and Val372 emulated by small molecule mitofusin activators according to the pharmacophore representation<sup>15,16</sup> were modeled according to the available protein structural information (Figure S5). Compared to **14B**, **14A** has an increased overlap with Leu57. In order for the amide carbonyl to occupy a space similar to Met376, the *trans* (1*r*,4*r*)-4-hydroxycyclohexyl-1-amino group is oriented in such a way that it causes an improbable overlap with Leu57. This steric crowding is likely to interfere with the ability of **14A** to interact with the proposed adjacent peptide. The direction of rotation with respect to the phenyl moiety caused by the {*R,R*} cyclopropyl bridging group in **14B** better accommodates and avoids this critical steric hindrance.

#### Improved Nervous System Accumulation of **5B**.

Because the potential clinical application of small molecule peptidomimetic mitofusin activators is neurological disorders,<sup>15,17</sup> **5B** levels were measured in plasma and brain tissues

at increasing times after a single 50 mg/kg oral dose. Plasma pharmacokinetics after oral **5B** administration were similar to those of the **5** isomeric mixture given at an identical dose and route in the same vehicle (10% DMSO, 90% [30% HP-*b*-CD]):  $t_{\max}$  for both was 0.5 h,  $t_{1/2}$  were 2.83 and 3.02 h, and mean tissue residence times (MRT) were 3.96 and 3.58 h, respectively (Table 3; compare with **5** values in Table 2) (Figure 9A). The calculated brain/plasma partition coefficient ( $AUC_{\text{brain}}/AUC_{\text{plasma}}$ ; Table 3) was 39.4%, *i.e.*,  $\sim$ 4-fold greater than previously reported for **2**.<sup>16</sup>

The normal central nervous system (brain and spinal cord) is protected by a semipermeable blood–brain barrier (BBB) that impedes the nonselective solute transport into the cerebrospinal fluid. The blood nerve barrier (BNB) serves as an analogous function for peripheral nerves<sup>22</sup> but is uniquely permeable at the dorsal root ganglia (DRG) that contain peripheral sensory nerve bodies.<sup>23</sup> This raised the possibility that small hydrophobic molecules like **5B** can gain access to peripheral nerves through DRGs and be concentrated therein, with therapeutic implications for treating neuropathies. Accordingly, **5B** levels were compared in the brain and spinal cord (parts of the central nervous system protected by the BBB) and both sciatic nerves (large peripheral nerves innervating the lower limbs that carry sensory neurons originating in DRGs). As reported in Table 3 and depicted in Figure 9B, **5B**  $C_{\max}$ , AUC,  $t_{1/2}$ , and mean residence time (MRT) were similar in all three neurological tissues. Indeed, the variance between the left and right sciatic nerves and the central and peripheral nervous systems was similar. These results do not indicate a meaningful effect of “leaky” DRG BNBs on peripheral nerve levels of this mitofusin activator.

The above results suggested that **5B** might exhibit favorable nervous system pharmacodynamics. Previous studies on mitofusin activators measured disease-relevant pharmacodynamic effects as a reversal of mitochondrial dysmotility in mouse disease model sciatic nerve axons<sup>15,17</sup> (Figure 10A). Peak mitochondrial motility after “burst” mitofusin activation with **2** reportedly occurred 4 h after administration and was completely extinguished after 24 h. By contrast, the peak mitochondrial motility after oral administration of **5B** occurred at 12 h, and benefits were maintained for greater than 24 h (Figure 10A–C). Perhaps, as a consequence of these favorable pharmacokinetic and pharmacodynamic properties, **5** partially ameliorated neuromuscular dysfunction in murine amyotrophic lateral sclerosis caused by a mutation of the superoxide

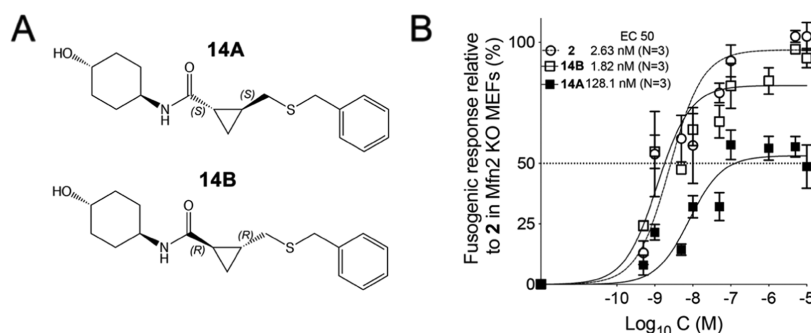


**Figure 6.** Mitochondrial fusogenic activities of **5** sulfide analogues. (A) Structures of **5** sulfide analogues synthesized for X-ray diffraction studies. (B) Dose–response curves showing **14B** (slower eluting isoform:  $EC_{50}$  = 1.82 nM; 95% confidence limits, 1.04–2.99 nM) and **14A** (faster eluting isoform:  $EC_{50}$  = 128.1 nM; 95% confidence limits,  $\sim$ 141.94 nM), increasing the mitochondrial aspect ratio (length/width) in cultured fibroblasts lacking Mfn2. Data are means  $\pm$  SEM from three independent experiments. **1** dose–response is shown for comparison ( $EC_{50}$  = 2.63 nM; 95% confidence limits, 1.45–4.64 nM).

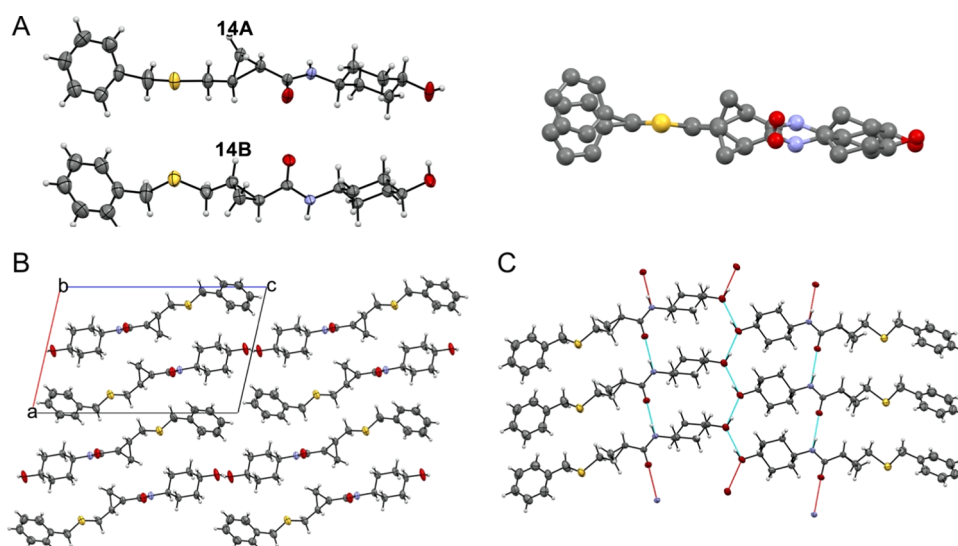


**Figure 7.** SCXRD structures of **14A** and **14B**. (A) (left) ORTEP diagrams of **14A** (inactive) and **14B** (active). Thermal ellipsoids are shown at 50% confidence intervals. Hydrogen atoms are geometrically idealized. (right) Superposition of **14A** and **14B** showing mirror structures. Hydrogen atoms are omitted for clarity. (B) Packing diagram viewed along the *b*-axis. Unit cell axes are shown and labeled. (C) Hydrogen-bonding interactions for **14B**. Complete hydrogen bonds are shown in blue; red bonds indicate that only one participating atom is present in the pictured molecules.

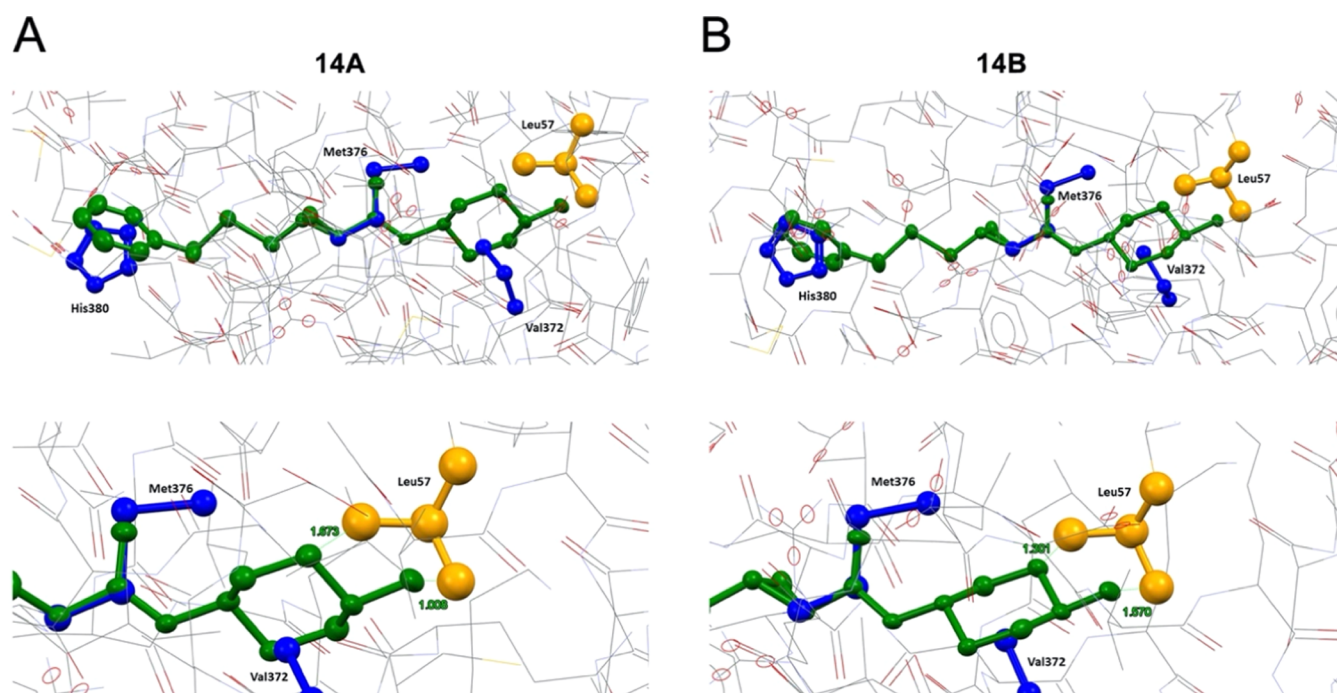


**Figure 8.** MFN2 peptide mimicry of 5 sulfide analogue enantiomers. (Top) Superimposition of compound enantiomers ((A) **14A** and (B) **14B**; both are green) onto human MFN2 residues Val372, Met376, and His380 (blue) are modeled as shown in Figure S5. MFN2 Leu57 is shown in orange. (Bottom) Close-up of modeled interactions between compound enantiomers and MFN2 Leu57. Human Mfn2 protein structure was computationally modeled in a closed configuration based on structural homology with human Mfn1 (PDB ID: 5GNS) and Arabidopsis thaliana dynamin-related protein (PDB ID: 3T34).

dismutase 1 (SOD1<sup>24</sup>), whereas **2** showed no significant benefit (Figure 10D).

Stimulation of mitochondrial motility in murine ALS by **5** was delayed in onset, and of longer than expected duration, based on its plasma (and brain, *vide infra*) levels (Figure 10B). This finding is consistent with the idea that facilitating mitochondrial motility is an indirect effect of mitofusins, mediated *via* their interactions with Miro proteins that couple

mitochondria to the Milton/Trak-dynein/kinesin transport apparatus.<sup>26,27</sup> Mitofusin regulation of mitochondrial fusion, motility, and mitophagy is mediated by mitofusin interactions with different effector proteins.<sup>28</sup> It seems likely that mitofusin recruitment of Miro proteins to function-critical subcellular domains or an essential multimolecular complex is the mechanism by which it facilitates mitochondrial coupling to the subcellular transport apparatus. Both Miro recruitment

Table 3. Pharmacokinetic Properties of 5B in Plasma and Nerve Tissues<sup>a</sup>

compound	tissue	dose route	actual mean dosage (mg/kg)	$t_{1/2}$ (h)	$t_{max}$ (h)	$C_{max}$ (ng/mL)	$AUC_{last}$ (h·ng/mL)	$MRT_{inf}$ (h)
5B	plasma	PO	50	2.83	0.50	12 100	34 000	3.96
	brain	PO	50	3.13	0.50	4030	13 400	4.30
	spinal cord	PO	50	2.71	0.50	4060	12 700	3.93
	left sciatic nerve	PO	50	3.21	0.50	4570	15 300	4.62
	right sciatic nerve	PO	50	2.61	0.50	5370	13 800	3.35

<sup>a</sup>Studies were performed in nonfasted mice, resulting in lower plasma 5B levels than reported after the same oral dose in fasted mice (see Table 4).

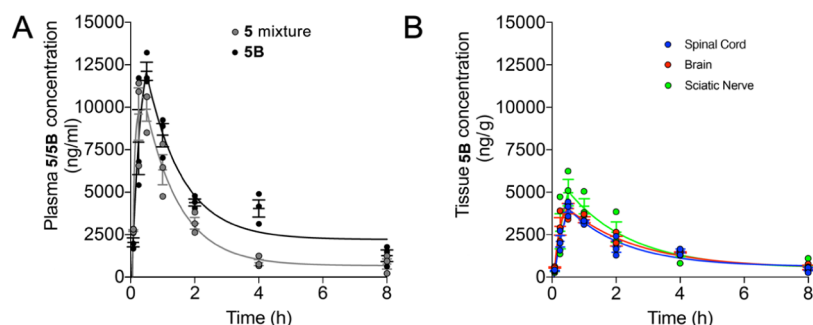


**Figure 9.** Plasma and tissue pharmacokinetics of 5B after oral administration to nonfasted mice. (A) Plasma pharmacokinetics of 5 isomeric mixture vs 5B in mice after a single oral dose of 50 mg/kg. (B) Comparative neuronal tissue concentrations of 5B after a single oral dose of 50 mg/kg. Vertical axis values are the same as in panels (A) and (B). Data are means  $\pm$  SEM; each dot represents one mouse. Calculated values are in the text.

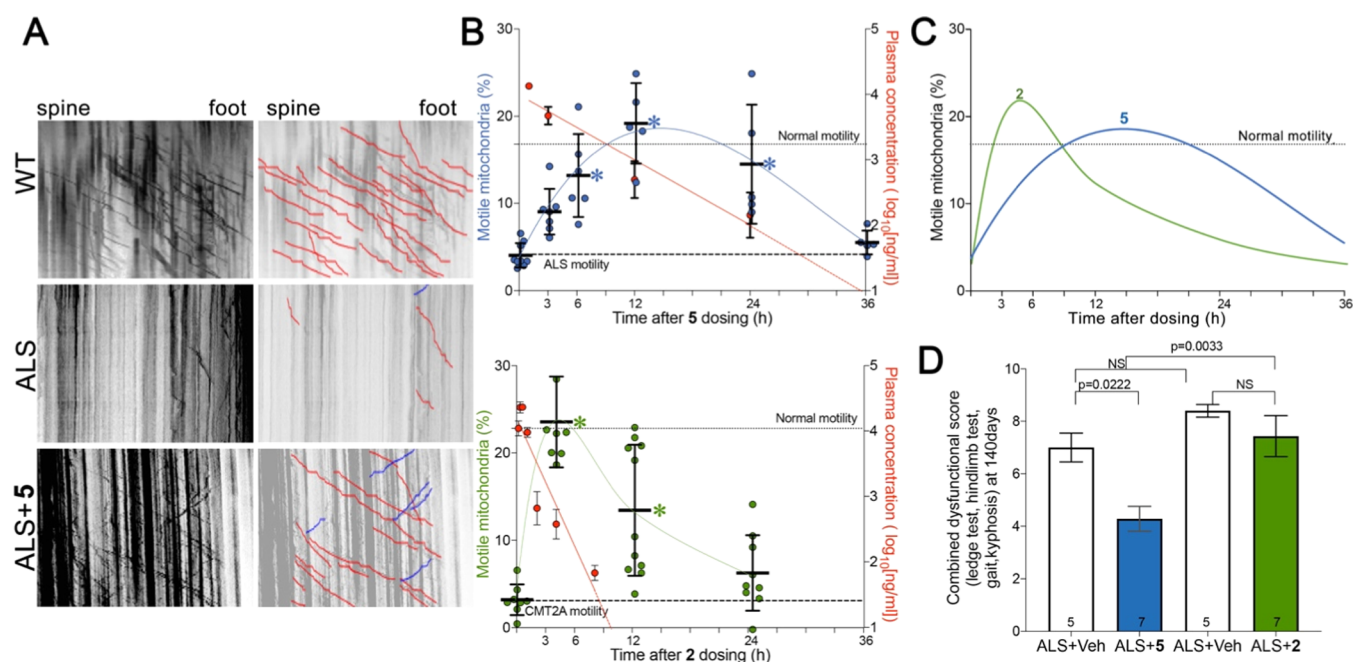


**Figure 10.** Pharmacodynamic and therapeutic effects of 5 vs 2 in murine ALS. (A) Representative kymographs for wild-type (WT) and ALS SOD1G93A mice (ALS) 12 h after oral administration of 5 or vehicle. (B) Time-dependent pharmacokinetics/pharmacodynamics of 5 and 2 after single oral doses (60 mg/kg). (Top) Blue values and left vertical axis show mitochondrial motility after 5 in ALS mouse sciatic nerve axons. (Bottom) Green values and left vertical axis show mitochondrial motility in CMT2A mouse sciatic nerve axons. Each point represents a single neuronal axon from two or three mice per time point. Red values and right vertical axes of the top graph show corresponding plasma 5 levels ( $n = 5$  per time point; means  $\pm$  SD); plasma levels of 2 are from ref 17. The dotted line designated “normal motility” is the mean value for WT in panel A; the dashed line designated “ALS motility” is the mean value for untreated ALS in panel A. (C) Comparative pharmacodynamics of 5 (blue) and 2 (green). (D) Effects of 5 (blue) and 2 (green) on the neuromuscular dysfunction score (ledge test, hindlimb test, gait, kyphosis<sup>25</sup>) in a proof-of-concept study of ALS mice.  $P$  values by ANOVA.

upon mitofusin activation and its restoration to baseline after mitofusin inactivation would take time. This can explain the observed temporal discontinuity between mitofusin activator pharmacokinetics and pharmacodynamics.

Together, the above results support superiority of 5 over 2 for extended pharmacodynamic effects and potential therapeutic values in experimental ALS. To better understand the underlying mechanisms, we performed a side-by-side compar-

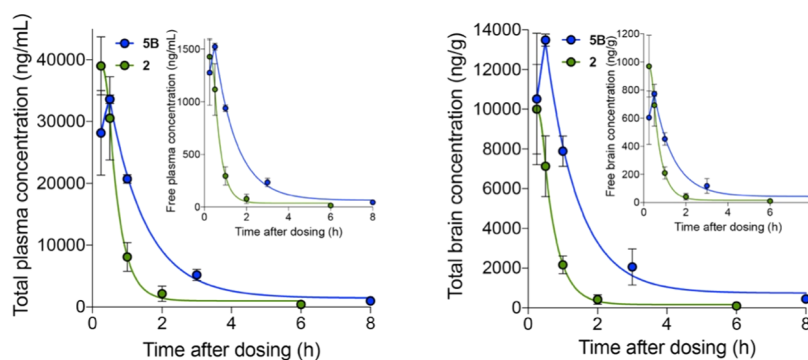


**Figure 11.** Comparative pharmacokinetic properties of **5B** and **2** in fasted mice. Left panel, total compound levels in plasma for **2** (green) and **5B** (blue); the inset shows free concentrations. Right panel, total brain compound levels; the inset shows free concentrations. Means  $\pm$  SEM of three mice per time point. Calculated values are in Table 4.

ison of **5B** and **2** plasma and brain pharmacokinetics. For these comparative studies, the two compounds were administered at the same dose (50 mg/kg) and route (oral gavage) and using the same vehicle (5 mg/mL in 30% SBE- $\beta$ -CD). As shown in Figure 11 and Table 4, greater brain bioavailability (total and free AUCs) and longer plasma and brain  $t_{1/2s}$  and MRTs were exhibited by **5B**.

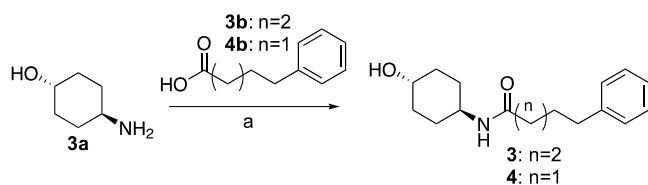
**Table 4. Comparative Plasma and Brain Pharmacokinetic Properties of Parent 2 and Lead Compound 5B in Fasting Mice<sup>a</sup>**

	Cpd 2 (50 mg/kg PO)		Cpd 5B (50 mg/kg PO)	
	total plasma	free plasma	total plasma	free plasma
$C_{max}$ (ng/mL)	39 011	1428	33 619	1523
$t_{1/2}$ (h)	1.280		1.67	
AUC <sub>0-last</sub> (ng·h/mL)	30 612	1121	59 567	2697
MRT <sub>0-last</sub> (h)	1.01		1.92	
	total brain	free brain	total brain	free brain
$C_{max}$ (ng/g)	10 001	970	13 480	774
$t_{1/2}$ (h)	0.999		1.77	
AUC <sub>0-last</sub> (ng·h/g)	7392	717	23 465	1347
MRT <sub>0-last</sub> (h)	0.959		1.98	

<sup>a</sup>Free compound concentrations were calculated from protein binding assays: **2**, mouse plasma 96.7%, mouse brain 90.3%; **5B**, mouse plasma 95.5%, mouse brain 94.3%.

**Chemistry.** Synthesis of **1** and **2** was previously described.<sup>15,16</sup> Synthesis of novel compounds **3–14** was accomplished, as outlined in Schemes 1–5. **3** and **4** were formed by the coupling of commercially available trans-4-aminocyclohexan-1-ol with 5-phenylpentanoic acid or 4-phenylpentanoic acid, as shown in Scheme 1.

**Scheme 1. Synthesis of 3 and 4<sup>a</sup>**



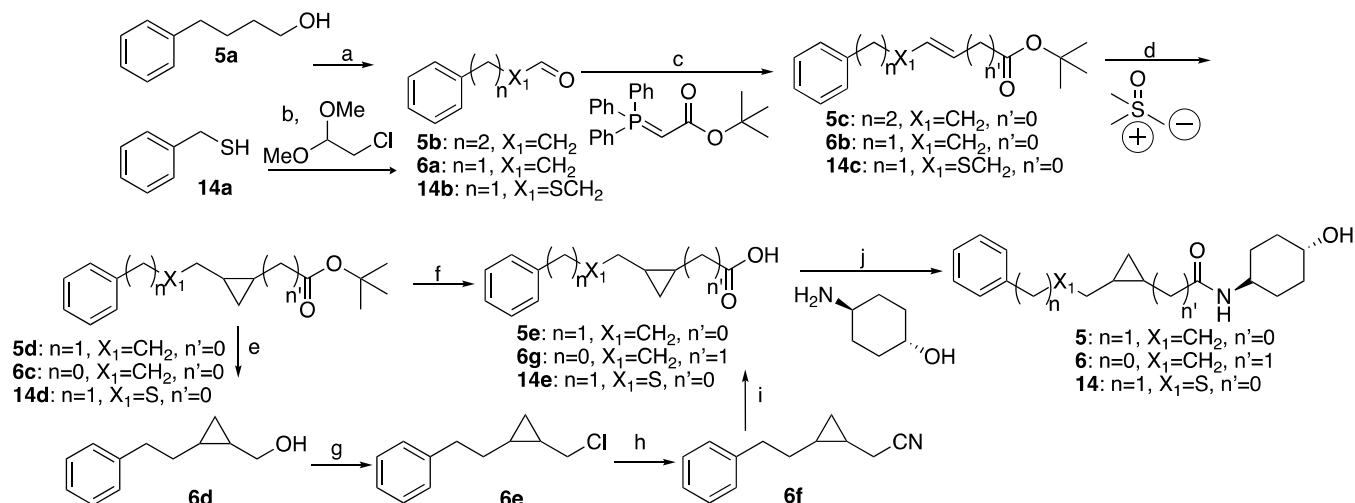
<sup>a</sup>Reagents and conditions: HATU, Et<sub>3</sub>N, THF, 25 °C, 2 h.

Scheme 2 includes compounds **5**, **6**, and **14**. Compounds **5** and **14** were synthesized by similar procedures but with the replacement of intermediate **5b** with sulfide **14b**. For compounds **5** and **14**, the last two steps (d and e) to the acid hydrolysis and amide condensation were accomplished by normal conditions from compounds **5d**, and **14d**. These were obtained from the Corey–Chaykovsky cyclopropanation reaction from compounds **5c** and **14c**. In turn, they were obtained from Wittig coupling with compounds **5b** and **14b**. Compound **5b** was formed by oxidation of **5a**. The sequence for compound **6** was similar but had some distinct differences. Aldehyde **6a** needed for coupling with the Wittig reagent was commercially available. Following similar cyclopropanation of **6b**, ester **6c** was reduced to afford alcohol **6d**, which was elongated *via* sequential formation of chloride **6e**, followed by cyanation to yield **6f**. Hydrolysis of nitrile **6f** yielded acid **6g** needed for the final amide coupling step, affording **6**.

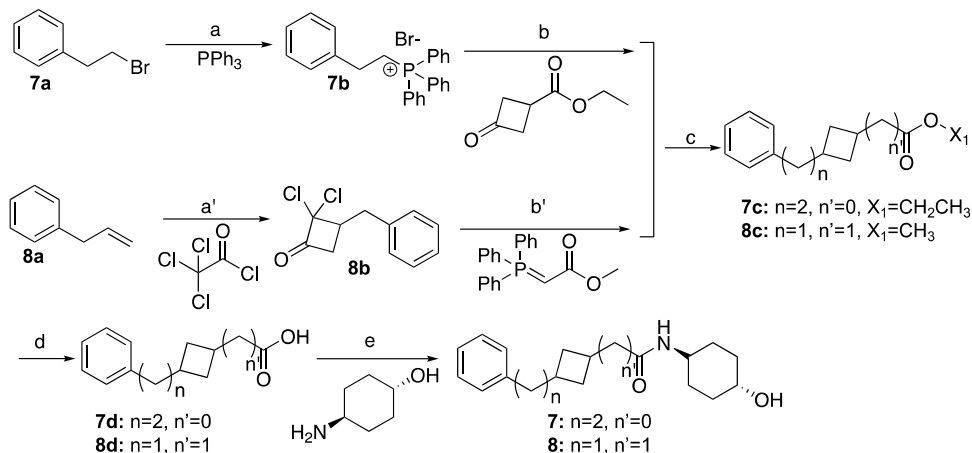
**7** and **8** were synthesized as shown in Scheme 3. Preparation of **7** commenced with the commercially available bromide **7a**, which was converted to the Wittig reagent **7b** *via* reaction with triphenylphosphine. Reaction of **7b** *via* treatment with sodium *t*-butoxide afforded the intermediate ylide, which was coupled with ethyl 3-oxocyclobutane-1-carboxylate to afford **7c**. This intermediate was converted to the final drug candidate **7** by hydrolysis of the ester to an intermediate acid followed by amide formation under standard conditions. Preparation of **8** began by formation of **8b** *via* zinc–copper-mediated coupling of trichloroacetyl chloride with 2-propen-1-ylbenzene **8a**. Removal of the chlorines by treatment with zinc in acetate acid followed by Wittig coupling afforded intermediate **8c**, which was converted to **8**, similar to procedures done for **7c** to **7**.

**9** and **10** were synthesized as shown in Scheme 4. Compound **9** was synthesized starting with the commercially available diester **9a** *via* alkaline hydrolysis to obtain acid **9b**, which was reduced by reaction with borane to afford alcohol **9c**. That alcohol was oxidized with the Dess–Martin periodinane to yield aldehyde **9d**, which was coupled with Wittig reagent **9e** to yield an intermediate olefin that was reduced with Pd/C under H<sub>2</sub> to obtain ester **9f**. This was hydrolyzed to afford acid **9g** that upon coupling with the 4-amino-cyclohexanol afforded **9**. Compound **10** was synthesized starting with the commercially available **10a** through similar procedures with **9d–9** to obtain **10**.

**11–13** were synthesized as shown in Scheme 5. Preparation of **11** began with the commercially available carboxylic acid

Scheme 2. Synthesis of **5**, **6**, and **14**<sup>a</sup>

<sup>a</sup>Reagents and conditions: (a) oxalyl chloride, dimethyl sulfoxide (DMSO), triethylamine (TEA), dichloromethane (DCM),  $-55$ – $25$  °C, 20 min. (b) (i) EtOH, EtONa, KI; (ii) 2-chloro-1,1-dimethoxyethane, 80 °C, 12 h; H<sub>2</sub>O, H<sub>2</sub>SO<sub>4</sub>, 60 °C, 12 h. (c) Tetrahydrofuran (THF), 20 °C. **5**, **14**: 12 h, **6**: 1 h. (d) NaH, DMSO, 20 °C, 1.5 h. (e) LiAlH<sub>4</sub>, THF, 0–25 °C, 3 h. (f) TFA, DCM, 25 °C, 15 h. (g) SOCl<sub>2</sub>, TEA, CHCl<sub>3</sub>, 0–70 °C, 1 h. (h) N(*n*Bu)<sub>4</sub>CN, THF, 70 °C, 12 h. (i) KOH, EtOH, H<sub>2</sub>O, 100 °C, 16 h. (j) HOBt, *N*-ethyl-*N'*-(3-dimethylaminopropyl)carbodiimide hydrochloride (EDCI), *N,N*-diisopropylethylamine (DIEA), DMV, 25 °C. **5**, **6**: 16 h, **14**: 2 h.

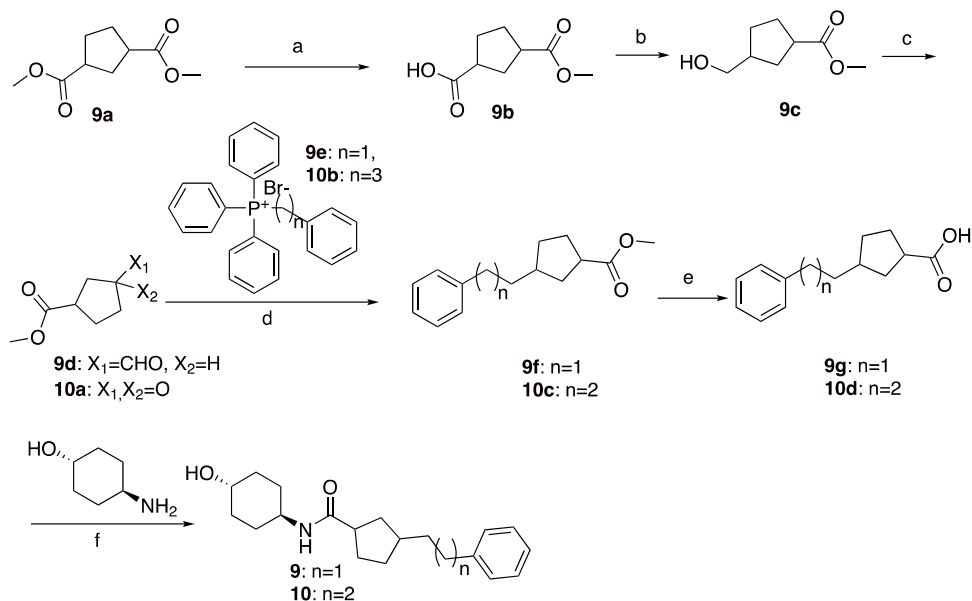
Scheme 3. Synthesis of **7** and **8**<sup>a</sup>

<sup>a</sup>Reagents and conditions: (a) 100 °C, 16 h. (b) Sodium 2-methylbutan-2-olate, toluene, 20–70 °C, 4.5 h. (a') Zinc–copper couple, Et<sub>2</sub>O, 20–35 °C, 18 h. (b') Acetic acid, zinc, 25–80 °C, 3 h, toluene, 110 °C, 2 h. (c) H<sub>2</sub>, Pd/C. **7**: EtOH, 20 °C, 16 h. **8**: MeOH, 25 °C, 2 h. (d) LiOH·H<sub>2</sub>O, MeOH/THF/H<sub>2</sub>O. **7**: 20 °C, 2 h. **8**: 25 °C, 16 h. (e) HOBt, EDCI, DIPEA, DMF, 16 h. **7**: 20 °C, **8**: 25 °C.

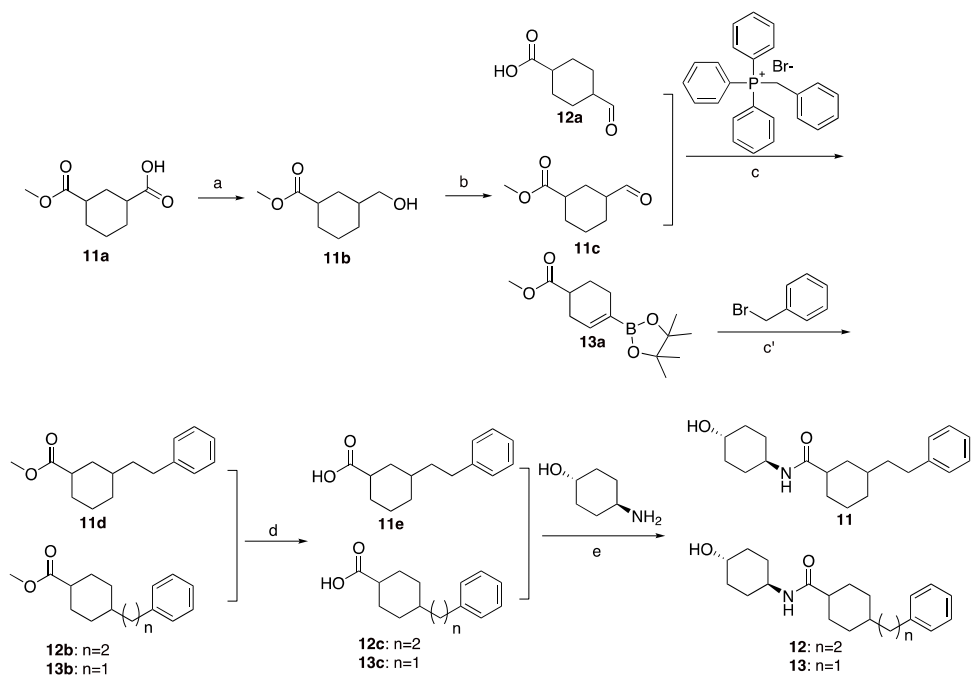
**11a**, which was reacted with borane-dimethylsulfide to obtain **11b**. Oxidation of **11b** to aldehyde **11c** was affected with pyridine sulfur trioxide, which after coupling with benzyl-(triphenyl)phosphonium bromide afforded olefin **11d**. Hydrogenation of this over Pd/C followed by hydrolysis yielded the penultimate acid **11e**, coupling of which with 4-amino-cyclohexanol afforded target **11**. Following a similar sequence, **12** was synthesized by starting with the commercially available 4-formylcyclohexane-1-carboxylic acid (**12a**). Compound **13** was made starting with the Suzuki coupling of methyl 4-(4,4,5,5-tetramethyl-1,3,2-dioxaborolan-2-yl)cyclohex-3-ene-1-carboxylate (**13a**) with benzylbromide followed by hydrogenation to afford **13b**. This intermediate was converted to **13**, similar to procedures done for **11d** and **12b**.

## CONCLUSIONS

In summary, rational redesign of 6-phenylhexanamide mitofusin activators incorporating cycloalkyl-containing linkers generated novel fusogenic compounds having improved pharmaceutical properties. Preclinical lead compound **5**, containing a cyclopropyl group in the linker, exhibited potent, stereoselective mitofusin activation. Single-crystal X-ray diffraction studies conducted with sulfide analogues of **5A** and **5B** showed that MFN2 interactions and biological activity reside exclusively in the *trans*-(*R,R*) enantiomer. The structural characteristics of **5B** are consistent with mitofusin activation through the physicochemical mimicry of human MFN2 Val372, Met376, and His380, *i.e.*, the function-critical amino acids in the progenitor mitofusin agonist peptide,<sup>14</sup> and provide further support for pharmacophore-based rational design of small molecule mitofusin activators. Compared to

Scheme 4. Synthesis of **9** and **10**<sup>a</sup>

<sup>a</sup>Reagents and conditions: (a) NaOH, MeOH, 25 °C, 12 h. (b) BH<sub>3</sub>-Me<sub>2</sub>S, THF, -78–25 °C, 12.5 h. (c) Dess–Martin, DCM, 25 °C, 2 h. (d) (i) *t*-BuOK, **9**: -20 °C, 2 h, **10**: toluene, 70 °C, 17 h. (ii) Pd/C, H<sub>2</sub>, MeOH, 25 °C, **9**: 2 h, **10**: 4 h. (e) LiOH·H<sub>2</sub>O, MeOH, THF, H<sub>2</sub>O, **9**: 25–70 °C, 2 h, **10**: 70 °C, 3 h. (f) HATU, Et<sub>3</sub>N, THF, 25 °C, **9**: 12 h, **10**: 16 h.

Scheme 5. Synthesis of **11**–**13**<sup>a</sup>

<sup>a</sup>Reagents and conditions: (a) BH<sub>3</sub>-SMe<sub>2</sub>, THF, -78–25 °C, 12.5 h. (b) Pyridine sulfur trioxide, Et<sub>3</sub>N, DMSO, 25 °C, 12 h. (c) (i) THF, *t*-BuOK, N<sub>2</sub>, -20 °C, 2 h, (ii) Pd/C, H<sub>2</sub>, MeOH, 25 °C, 2 h. (c') (i) Pd(dppf)Cl<sub>2</sub>, dioxane, H<sub>2</sub>O, K<sub>2</sub>CO<sub>3</sub>, N<sub>2</sub>, 25–100 °C, 2 h. (ii) Pd/C, H<sub>2</sub>, MeOH, 25 °C, 2 h. (d) LiOH·H<sub>2</sub>O, MeOH, THF, H<sub>2</sub>O, 25–70 °C, 2 h. (e) HATU, Et<sub>3</sub>N, THF, 25 °C, 12 h.

parent compound **2**, **5B** exhibited sustained brain levels, markedly prolonged pharmacodynamic effects, and disease modification in a proof-of-concept study of murine amyotrophic lateral sclerosis. Thus, **5B** is a strong candidate for preclinical evaluation in diseases, wherein sustained activation of mitofusin-mediated mitochondrial fusion and transport might counteract neurological degeneration.

## EXPERIMENTAL SECTION

**General Procedures and Instrumentation.** Compounds are at least 95% pure by HPLC (column: Kinetex C18 LC, 4.6 mm × 50 mm, 5 μm; mobile phase A: 0.0375% TFA in water (v/v), B: 0.01875% TFA in acetonitrile (v/v)) run at 50 °C with absorbance at 200 nM peaks.

LC-MS/MS (ESI) was performed using multiple systems: (1) SHIMADZU LC-MS-2020 with LabSolution V5.72 analysis software,

HPLC used a Chromalith@Flash RP-18E 25 mm × 2.0 mm column ran at 50 °C with a PDA (220 and 254 nm) detector, acquired data in the scan MS mode (positive mode) with  $m/z = 100$ – $1000$  scan range, drying gas (N<sub>2</sub>) flow: 15 L/min, DL voltage: 120 V, and Quarry DC voltage: 20 V. (2) Agilent 1200/G6110A instrument with AgilentChemStation Rev. B. 04.03 software. HPLC used an Xbridge C18 2.1 mm × 50 mm, 5 μm column ran at 40 °C with a DAD (220 nm)/ELSD detector, acquired data in the scan MS mode (positive mode) with  $m/z = 100$ – $1000$  scan range, drying gas (N<sub>2</sub>) flow: 10 L/min, 350 °C, nebulizer pressure: 35 psi, capillary voltage: 2500 V. NMR spectrometry was carried out on a Bruker AVANCE NEO 400 MHz with a 5 mm PABBO BB/19F-1H/D Z-GRD probe.

#### Synthesis and Characterization of Compounds 1–14.

Compounds were synthesized and analyzed at WuXi Aptec Co. Ltd. NMR, analytical HPLC, and LC-MS were reported previously. All starting reagents not reported are known compounds purchased by WuXi Aptec Co. Ltd., from third-party suppliers. The synthesis procedure for compounds 1–2 was reported previously.<sup>16</sup>

*N*-(1*r*,4*r*)-4-Hydroxycyclohexyl)-5-phenylpentanamide (3). To a mixture of trans-4-aminocyclohexan-1-ol (3a, 500 mg, 4.34 mmol, 1.00 equiv) and 5-phenylpentanoic acid (3b, 928 mg, 5.21 mmol, 1.20 equiv) in THF (10.0 mL) were added HATU (2.48 g, 6.51 mmol, 1.50 equiv) and Et<sub>3</sub>N (1.32 g, 13.0 mmol, 1.81 mL, 3.00 equiv) in one portion at 25 °C. The mixture was stirred at 25 °C for 2 h. TLC showed that the reaction was completed. TLC indicated (petroleum/ethyl acetate = 3:1) that some compound 2a ( $R_f = 0.14$ ) remained, and one major new spot with larger ( $R_f = 0.29$ ) polarity was detected. The reaction mixture was diluted with 50.0 mL of H<sub>2</sub>O and extracted with 60.0 mL of ethyl acetate (20.0 mL × 3). The combined organic layers were washed with 60.0 mL of brine (20.0 mL × 3), dried over [Na<sub>2</sub>SO<sub>4</sub>], filtered, and concentrated under reduced pressure to give a residue. The crude product was purified by reversed-phase HPLC (0.1% NH<sub>3</sub>-H<sub>2</sub>O). 3 (106.02 mg, 0.38 mmol, 8.87% yield) was obtained as a white solid. LC-MS: RT = 0.851 min,  $m/z = 276.4$  (M + H)<sup>+</sup>. HPLC: RT = 1.75 min, 98.7% purity, under 220 nm. SFC: RT = 1.14 min, ee% = 100%, under 220 nm. <sup>1</sup>H NMR: (400 MHz, MeOD) δ 7.25–7.22 (m, 2H), 7.16–7.13 (m, 3H), 3.62–3.59 (m, 1H), 3.51–3.49 (m, 1H), 2.62–2.59 (m, 2H), 2.18–2.14 (m, 2H), 1.92–1.88 (m, 4H), 1.63–1.59 (m, 4H), 1.32–1.27 (m, 4H).

*N*-(1*r*,4*r*)-4-Hydroxycyclohexyl)-4-phenylbutanamide (4). A mixture of trans-4-aminocyclohexan-1-ol (3a, 300 mg, 2.60 mmol, 1.00 equiv), 4-phenylbutanoic acid (4b, 513 mg, 3.13 mmol, 1.20 equiv), Et<sub>3</sub>N (790 mg, 7.81 mmol, 1.09 mL, 3.00 equiv), and HATU (1.49 g, 3.91 mmol, 1.50 equiv) in THF (10.0 mL) was stirred at 25 °C for 2 h. TLC indicated (petroleum/ethyl acetate = 3:1) that some compound 2 ( $R_f = 0.12$ ) remained, and one major new spot with larger ( $R_f = 0.26$ ) polarity was detected. The reaction mixture was diluted with 50.0 mL of H<sub>2</sub>O and extracted with 60.0 mL of ethyl acetate (20.0 mL × 3). The combined organic layers were washed with 60.0 mL of brine (20.0 mL × 3), dried over [Na<sub>2</sub>SO<sub>4</sub>], filtered, and concentrated under reduced pressure to give a residue. The crude product was purified by reversed-phase HPLC (0.1% NH<sub>3</sub>-H<sub>2</sub>O). 4 (108.64 mg, 0.42 mmol, 15.9% yield) was obtained as a white solid. LC-MS: RT = 0.820 min,  $m/z = 262.3$  (M + H)<sup>+</sup>. HPLC: RT = 1.604 min, 97.2% purity, under 220 nm. SFC: RT = 1.05 min, ee% = 100%, under 220 nm. <sup>1</sup>H NMR (400 MHz, MeOD) δ 7.27–7.23 (m, 2H), 7.18–7.15 (m, 3H), 3.61–3.60 (m, 1H), 3.53–3.50 (m, 1H), 2.62–2.58 (m, 2H), 2.18–2.14 (m, 2H), 1.92–1.87 (m, 6H), 1.36–1.24 (m, 4H).

*N*-(4-Hydroxycyclohexyl)-2-(3-phenylpropyl)cyclopropane-1-carboxamide (5). To a solution of oxalyl chloride (4.65 g, 36.6 mmol, 3.20 mL, 1.10 equiv) in DCM (75.0 mL) was cooled to –55 °C under a N<sub>2</sub> atmosphere was added dropwise a solution of DMSO (5.72 g, 73.2 mmol, 5.72 mL, 2.20 equiv) in DCM (30.0 mL) was, after stirring for 5 min, dropwise added 4-phenylbutan-1-ol (5a, 5.00 g, 33.2 mmol, 5.08 mL, 1.00 equiv) in DCM (15.0 mL) was added dropwise, after stirring for 15 min, TEA (16.8 g, 166 mmol, 23.1 mL, 5.00 equiv) was added, then it was warmed to 25 °C. At that point, 100 mL of 1 N HCl was added and the suspension was extracted with 200 mL of DCM (100 mL × 2). The combined organic layers were

washed with 50 mL of water, dried over Na<sub>2</sub>SO<sub>4</sub>, filtered, and concentrated to give 4-phenylbutanal (5b, 5.00 g). To a solution of 5b (5.00 g, 33.7 mmol, 9.80 mL, 1.00 equiv) in THF (50.0 mL) was added *tert*-butyl 2-(triphenyl-λ<sup>5</sup>-phosphanyliden)acetate (16.5 g, 43.8 mmol, 1.30 equiv) and stirred at 20 °C for 12 h to give *tert*-butyl (E)-6-phenylhex-2-enoate (5c, 6.00 g, 24.3 mmol, 72.1% yield). To a solution of NaH (1.17 g, 29.2 mmol, 60.0% purity, 1.20 equiv) in DMSO (30.0 mL) was added dimethylmethanesulfonic iodide (6.43 g, 29.2 mmol, 1.20 equiv) and the mixture was stirred at 20 °C for 0.5 h, and then 5c (6.00 g, 24.3 mmol, 1.00 equiv) in DMSO (3.00 mL) was added and stirred at 20 °C for 1 h to give *tert*-butyl 2-(3-phenylpropyl)cyclopropane-1-carboxylate (5d, 2.10 g, 8.07 mmol, 33.1% yield). TFA (7.70 g, 67.5 mmol, 5.00 mL, 17.5 equiv) was added to a solution of 5d (1.00 g, 3.84 mmol, 1.00 equiv) in DCM (5.00 mL) and stirred at 25 °C for 15 h to give 2-(3-phenylpropyl)cyclopropane-1-carboxylic acid (3e, 800 mg). EDCI (1.00 g, 5.22 mmol, 1.50 equiv), HOBt (564 mg, 4.18 mmol, 1.20 equiv), DIPEA (1.35 g, 10.4 mmol, 1.82 mL, 3.00 equiv), and 4-aminocyclohexan-1-ol (580 mg, 3.83 mmol, 1.10 equiv, HCl) were added to a solution of 3e (800 mg, 3.48 mmol, 1.00 equiv) in DMF (8.00 mL) and stirred at 25 °C for 16 h. The residue was purified by prep-HPLC (column: Waters Xbridge C18 150 mm × 50 mm × 10 μm; mobile phase: [water (10 mM NH<sub>4</sub>HCO<sub>3</sub>)-ACN]; B%: 28–58%, 11.5 min) to give 5 (110 mg, 361 μmol, 10.3% yield) as a white solid. LC-MS:  $R_t = 0.904$  min,  $m/z = 302.1$  (M + H)<sup>+</sup>. HPLC:  $R_t = 2.898$  min, purity: 98.6%, under 220 nm. <sup>13</sup>C NMR: (400 MHz MeOD) δ 173.97, 142.27, 127.96, 127.89, 125.31, 69.07, 35.14, 33.45, 32.23, 30.87, 30.24, 21.27, 20.55, 13.04. <sup>1</sup>H NMR: (400 MHz MeOD) δ 7.27–7.24 (m, 2H), 7.18–7.15 (m, 3H), 3.64–3.61 (m, 1H), 3.55–3.50 (m, 1H), 2.64 (t,  $J = 8$  Hz, 2H), 1.97–1.89 (m, 4H), 1.75–1.73 (m, 2H), 1.36–1.04 (m, 8H), 1.29–1.27 (m, 1H), 0.59–0.57 (m, 1H).

**Separation Method of 5A and 5B Isoforms from 5 Mixture Isoforms.** Thar 200 preparative SFC (SFC-7) with column (ChiralPak IG, 30050 mm I.D., 10 μm), mobile phase: A for CO<sub>2</sub> and B for methanol (0.1% NH<sub>3</sub>-H<sub>2</sub>O); gradient: B 35%; flow rate: 200 mL/min; back pressure: 100 bar column temperature: 38 °C; wavelength: 220 nm; cycle time: ~4 min; sample preparation: compound was dissolved in ~200 mL of methanol; injection: 10 mL per injection. After separation, the fractions were dried off *via* a rotary evaporator at a bath temperature of 40 °C to get the desired isoforms. 5A was the faster eluting isomer by SFC on IG column, and 5B was the slower eluting isomer. Waters UPC2 analytical SFC (SFC-H) with column (ChiralPak IG, 150 mm × 4.6 mm I.D., 3 μm); mobile phase: A for CO<sub>2</sub> and B for methanol (0.05%DEA); gradient: B 40%; flow rate: 2.5 mL/min; back pressure: 100 bar; column temperature: 35 °C; wavelength: 220 nm. LC-MS: 5A:  $R_t = 2.445$  min,  $m/c = 302.2$  (M + H)<sup>+</sup>, 5B:  $R_t = 2.445$  min,  $m/c = 302.2$  (M + H)<sup>+</sup>. SFC: 5A:  $R_t = 0.852$  min, 5B:  $R_t = 1.179$  min. <sup>13</sup>C NMR: 5A: (400 MHz MeOD) δ 173.97, 142.27, 127.96, 127.89, 125.31, 69.07, 35.14, 33.46, 32.24, 30.86, 30.24, 21.29, 20.55, 13.05. 5B: (400 MHz MeOD) δ 173.97, 142.28, 127.96, 127.90, 125.31, 69.07, 35.14, 33.45, 32.24, 30.86, 30.24, 21.29, 20.55, 13.05.

*N*-(4-Hydroxycyclohexyl)-2-(2-phenethylcyclopropyl)acetamide (6). *tert*-Butyl 2-(triphenyl-λ<sup>5</sup>-phosphanyliden)acetate (25.2 g, 67.0 mmol, 1.50 equiv) was added to a solution of 3-phenylpropanal (6a, 6.00 g, 44.7 mmol, 5.88 mL, 1.00 equiv) in THF (100 mL) and stirred at 20 °C for 1 h to give *tert*-butyl (E)-5-phenylpent-2-enoate (6b, 10.0 g, 42.1 mmol, 94.3% yield). Dimethylmethanesulfonic iodide (10.0 g, 45.5 mmol, 1.20 equiv) was added to a solution of NaH (1.82 g, 45.5 mmol, 60.0% purity, 1.20 equiv) in DMSO (45.0 mL), and the mixture was stirred at 20 °C for 0.5 h; then 6b (9.00 g, 37.9 mmol, 1.00 equiv) in DMSO (5.00 mL) was added, and the reaction mixture was stirred at 20 °C for 1 h to give *tert*-butyl 2-phenethylcyclopropane-1-carboxylate (6c, 6.00 g, 24.3 mmol, 64.1% yield). LiAlH<sub>4</sub> (924 mg, 24.3 mmol, 2.00 equiv) at 0 °C was added to a solution of 6c (3.00 g, 12.1 mmol, 1.00 equiv) in THF (45.0 mL), stirred at 25 °C for 3 h, and then the reaction mixture was cooled to 0 °C and 1.00 mL of water was dropwise added, then added 1.00 mL of 15.0% NaOH and 3.00 mL of water and warmed to 25 °C, stirred for 15

min, then added 20.0 g  $\text{MgSO}_4$  and stirred for 15 min to give (2-phenethylcyclopropyl)methanol (**6d**, 2.00 g, 10.1 mmol, 82.9% yield). A solution of (2-phenethylcyclopropyl)methanol (**6d**, 2.00 g, 10.1 mmol, 1.00 equiv) and TEA (2.04 g, 20.2 mmol, 2.81 mL, 2.00 equiv) in  $\text{CHCl}_3$  (20.0 mL) was cooled to 0 °C and  $\text{SOCl}_2$  (2.40 g, 20.2 mmol, 1.47 mL, 2.00 equiv) was added dropwise. The reaction mixture was stirred at 70 °C for 1 h. The organic phase was separated, the aqueous phase was extracted with 40.0 mL of DCM (20 mL  $\times$  2). The combined organic layers were washed with 20.0 mL of brine, dried over  $\text{Na}_2\text{SO}_4$ , filtered, and concentrated. The residue was purified by column chromatography ( $\text{SiO}_2$ , petroleum ether/ethyl acetate = 1/0, plate 2, petroleum ether/ethyl acetate = 1/0,  $R_f$  = 0.50) to give (2-(2-(chloromethyl)cyclopropyl)ethyl)benzene (**6e**, 1.80 g, 8.69 mmol, 86.0% yield). A solution of (2-(2-(chloromethyl)cyclopropyl)ethyl)benzene (**6e**, 1.80 g, 8.69 mmol, 1.00 equiv) in THF (9.00 mL) and  $\text{N}(\text{nBu})_4\text{CN}$  (2.80 g, 10.4 mmol, 1.20 equiv) was stirred at 70 °C for 12 h to give 2-(2-phenethylcyclopropyl)acetonitrile (**6f**, 1.40 g, 7.56 mmol, 86.9% yield); then, EtOH (7.00 mL),  $\text{H}_2\text{O}$  (7.00 mL), and KOH (1.70 g, 30.2 mmol, 4.00 equiv) were added and stirred at 100 °C for 16 h to give 1-(2-phenethylcyclopropyl)propan-2-one (**6g**, 1.50 g, 6.95 mmol, 92.0% yield). To a solution of 1-(2-phenethylcyclopropyl)propan-2-one (**6g**, 1.00 g, 4.64 mmol, 1.00 equiv) in DMF (10.0 mL) were added EDCI (1.33 g, 6.95 mmol, 1.50 equiv), HOBt (751 mg, 5.56 mmol, 1.20 equiv), DIPEA (1.80 g, 13.9 mmol, 2.42 mL, 3.00 equiv), and 4-aminocyclohexan-1-ol (773 mg, 5.10 mmol, 1.10 equiv, HCl); the mixture was stirred at 25 °C for 16 h; LC-MS showed that **6g** was consumed completely and desired MS ( $R_t$  = 0.882 min) was detected; the residue was purified by prep-HPLC (column: Waters Xbridge C18 150 mm  $\times$  50 mm  $\times$  10  $\mu\text{m}$ ; mobile phase: [water (10 mM  $\text{NH}_4\text{HCO}_3$ )-ACN]; B%: 28–58%, 11.5 min) to give **6** (99.35 mg, 329  $\mu\text{mol}$ , 7.11% yield, 100% purity) as a white solid. LC-MS:  $R_t$  = 0.895 min,  $m/z$  = 302.1 (M + H)<sup>+</sup>. HPLC:  $R_t$  = 2.803 min, purity: 100%, under 220 nm. <sup>13</sup>C NMR: (400 MHz MeOD)  $\delta$  173.58, 142.27, 128.05, 127.84, 125.25, 69.03, 40.16, 35.84, 35.34, 33.40, 30.14, 17.77, 15.15, 10.80. <sup>1</sup>H NMR: (400 MHz MeOD)  $\delta$  7.27–7.23 (m, 2H), 7.19–7.14 (m, 3H), 3.65–3.60 (m, 1H), 3.55–3.50 (m, 1H), 2.69 (t,  $J$  = 7.6 Hz, 2H), 2.09–2.02 (m, 2H), 1.97–1.89 (m, 4H), 1.75–1.73 (m, 1H), 1.51–1.49 (m, 1H), 1.38–1.30 (m, 4H), 0.82–0.80 (m, 1H), 0.64–0.53 (m, 1H), 0.37–0.32 (m, 2H).

**N-(4-Hydroxycyclohexyl)-3-phenethylcyclobutane-1-carboxamide (7).** A mixture of (2-bromoethyl)benzene (**7a**, 10.0 g, 54.0 mmol, 7.30 mL, 1.00 equiv) and triphenylphosphine (14.2 g, 54.0 mmol, 1.00 equiv) was stirred at 100 °C for 16 h and then cooled to 20 °C to give compound 2-phenethyl-triphenylphosphonium bromide (**7b**, 20.0 g, 44.4 mmol, 82.2% yield, 99.4% purity); to this were then added toluene (47.0 mL) and sodium 2-methylbutan-2-olate (1.16 g, 10.5 mmol, 1.50 equiv), and the mixture was stirred at 20 °C for 0.5 h under  $\text{N}_2$ , at which point a solution of ethyl 3-oxocyclobutane-1-carboxylate (1.00 g, 7.03 mmol, 1.00 equiv) in toluene (10.0 mL) was added dropwise to the mixture and the mixture was stirred at 70 °C for 4 h under  $\text{N}_2$  and then concentrated under reduced pressure to give a residue that was purified by reverse phase HPLC to give ethyl 3-(2-phenylethylidene)cyclobutane-1-carboxylate (0.30 g, 1.14 mmol, 16.2% yield, 87.7% purity); then, EtOH (24.0 mL) and Pd/C (0.24 g, 10.0% purity) were added under  $\text{N}_2$ , the suspension was degassed and purged with  $\text{H}_2$  for 3 times, the mixture was stirred at 20 °C for 16 h under  $\text{H}_2$  (15 psi), and then filtered through kieselguhr, and the filter residue was washed with ethyl acetate (60.0 mL); the layer was concentrated under reduced pressure to give ethyl 3-phenethylcyclobutane-1-carboxylate (**7c**, 1.10 g, 2.46 mmol, 47.1% yield, 51.9% purity). To a solution of ethyl **7c** (1.10 g, 2.46 mmol, 1.00 equiv) in MeOH (5.00 mL), THF (10.0 mL), and  $\text{H}_2\text{O}$  (5.00 mL) was added LiOH· $\text{H}_2\text{O}$  (412 mg, 9.83 mmol, 4.00 equiv), stirred at 20 °C for 2 h, the mixture was concentrated under reduced pressure to give a residue, the residue was poured into  $\text{H}_2\text{O}$  (30.0 mL) and extracted with ethyl acetate (30.0 mL  $\times$  2), the pH of the water phase was adjusted to 3–4 with 1 N HCl (10.0 mL) and extracted with ethyl acetate (50.0 mL  $\times$  3); the combined layers were dried over  $\text{Na}_2\text{SO}_4$ , filtered, and concentrated under reduced pressure to give 3-

phenethylcyclobutane-1-carboxylic acid (**7d**, 0.64 g, 1.79 mmol, 72.6% yield, 57.0% purity) as a yellow oil. To a solution of **7d** (0.64 g, 1.79 mmol, 1.00 equiv) in DMF (5.00 mL) were added HOBt (362 mg, 2.68 mmol, 1.50 equiv), EDCI (445 mg, 2.32 mmol, 1.30 equiv), DIPEA (692 mg, 5.36 mmol, 93  $\mu\text{L}$ , 3.00 equiv), and 4-aminocyclohexan-1-ol (325 mg, 2.14 mmol, 1.20 equiv, HCl) and stirred at 20 °C for 16 h. The mixture was purified by prep-HPLC (column: Waters Xbridge C18 150 mm  $\times$  50 mm  $\times$  10  $\mu\text{m}$ ; mobile phase: [water (10 mM  $\text{NH}_4\text{HCO}_3$ )-ACN]; B%: 28–58%, 11.5 min) to give **7** (111.58 mg, 370  $\mu\text{mol}$ , 20.7% yield, 100% purity) as a white solid. LC-MS:  $R_t$  = 0.813 min,  $m/z$  = 302.2 (M + H)<sup>+</sup>;  $R_t$  = 0.883 min,  $m/z$  = 302.1 (M + H)<sup>+</sup>. HPLC: purity: 100% under 220 nm. <sup>1</sup>H NMR: (400 MHz MeOD)  $\delta$  7.25–7.21 (m, 2H), 7.15–7.13 (m, 3H), 3.59–3.49 (m, 2H), 2.82–2.80 (m, 1H), 2.53–2.50 (m, 2H), 2.18–2.16 (m, 3H), 1.92–1.67 (m, 8H), 1.32–1.27 (m, 4H). <sup>13</sup>C NMR: (400 MHz MeOD)  $\delta$  177.895, 176.889, 143.747, 129.521, 129.422, 126.826, 70.621, 39.844, 39.737, 37.306, 35.031, 34.421, 32.781, 32.435, 31.676, 31.198.

**2-(3-Benzylcyclobutyl)-N-(4-hydroxycyclohexyl)acetamide (8).** To a solution of allylbenzene (**8a**) (20.0 g, 169 mmol, 22.4 mL, 1.00 equiv), zinc–copper couple (65.5 g, 508 mmol, 3.00 equiv) in  $\text{Et}_2\text{O}$  (200 mL) were added dropwise 2,2,2-trichloroacetyl chloride (61.6 g, 338 mmol, 37.8 mL, 2.00 equiv) and  $\text{POCl}_3$  (29.2 g, 190 mmol, 17.7 mL, 1.12 equiv) in  $\text{Et}_2\text{O}$  (100 mL) at 20 °C under  $\text{N}_2$  for 2 h, and then the reaction was stirred at 35 °C for 16 h; the mixture was filtered through a pad of celite, and the filtrate was poured into water (300 mL) and extracted with  $\text{Et}_2\text{O}$  (200 mL  $\times$  3); the organic layer was washed with saturated  $\text{NaHCO}_3$  (200 mL  $\times$  2) and brine (200 mL), dried over  $\text{Na}_2\text{SO}_4$ , filtered, and concentrated under reduced pressure to give 3-benzyl-2,2-dichlorocyclobutan-1-one (**8b**, 46.2 g). To a solution of zinc (52.8 g, 807 mmol, 4.00 equiv) in AcOH (120 mL) was added **8b** (46.2 g, 202 mmol, 1.00 equiv) in AcOH (120 mL) dropwise at 25 °C for 1 h, stirred at 25 °C for 1 h, and then heated at 80 °C for 1 h; the mixture was filtered and poured into water (200 mL), extracted with EtOAc (200 mL  $\times$  3); the organic layer was combined and washed with  $\text{NaHCO}_3$  (saturated, 150 mL  $\times$  2) and brine (200 mL), dried over  $\text{Na}_2\text{SO}_4$ , filtered, and concentrated under reduced pressure and was purified by reverse phase HPLC (0.1% FA condition) to get 3-benzylcyclobutan-1-one (14.8 g, 78.6 mmol, 38.9% yield, 85.0% purity); to a solution of 3-benzylcyclobutan-1-one (1.00 g, 5.31 mmol, 1.00 equiv) in toluene (20 mL) was added methyl 2-(triphenyl- $\text{P}^{\text{+}}$ -phosphanylidene)acetate (2.66 g, 7.96 mmol, 1.50 equiv) and stirred at 110 °C for 2 h; the reaction was concentrated under vacuum to get a residue and triturated with petroleum ether (20 mL) at 25 °C for 10 min; the product was purified by prep-HPLC (column: Phenomenex luna C18 150 mm  $\times$  40 mm  $\times$  15  $\mu\text{m}$ ; mobile phase: [water (0.225% FA)-ACN]; B%: 47–77%, 10 min) to get methyl 2-(3-benzylcyclobutylidene)acetate (943 mg, 4.34 mmol, 81.8% yield, 99.5% purity). To a solution of methyl 2-(3-benzylcyclobutylidene)acetate (943 mg, 4.34 mmol, 1.00 equiv) in MeOH (20 mL) was added Pd/C (0.20 g, 10% purity); the reaction was degassed and back-filled with  $\text{H}_2$  (15 psi) and stirred at 25 °C for 2 h; the residue was filtered through diatomite, and the filtrate was concentrated under vacuum to afford methyl 2-(3-benzylcyclobutyl)acetate (**8c**, 947 mg, 4.31 mmol, 99.2% yield, 99.3% purity); to a solution of **8c** (947 mg, 4.31 mmol, 1.00 equiv) in THF (10 mL),  $\text{H}_2\text{O}$  (5 mL) and MeOH (5 mL) was added LiOH· $\text{H}_2\text{O}$  (723 mg, 17.2 mmol, 4.00 equiv); the reaction mixture was stirred at 25 °C for 16 h, and then the reaction mixture was concentrated to get a residue and was poured into  $\text{H}_2\text{O}$  (15 mL) and extracted with EtOAc (15 mL  $\times$  3); the aqueous layer was adjusted to pH 2–3 and extracted with EtOAc (15 mL  $\times$  3), dried over  $\text{Na}_2\text{SO}_4$ , filtered, and concentrated under reduced pressure to give 2-(3-benzylcyclobutyl)acetic acid (**8d**, 877 mg, 4.05 mmol, 94.0% yield, 94.4% purity) as a light yellow oil. To a solution of **8d** (300 mg, 1.39 mmol, 1.00 equiv) in DMF (5 mL) were added HOBt (225 mg, 1.66 mmol, 1.20 equiv), EDCI (399 mg, 2.08 mmol, 1.50 equiv), DIEA (538 mg, 4.16 mmol, 724  $\mu\text{L}$ , 3.00 equiv), and aminocyclohexan-1-ol (241 mg, 1.53 mmol, 1.10 equiv, HCl). The reaction mixture was stirred at 25 °C for 16 h and poured into  $\text{H}_2\text{O}$

(15 mL) and extracted with EtOAc (10 mL  $\times$  3); the organic layer was dried over Na<sub>2</sub>SO<sub>4</sub>, filtered, and concentrated under reduced pressure to give a residue and was purified by prep-HPLC (column: Phenomenex luna C18 150 mm  $\times$  40 mm  $\times$  15  $\mu$ m; mobile phase: [water (0.225% FA)-ACN]; B%: 23–53%, 9 min) to get **8** (111.58 mg, 366  $\mu$ mol, 26.3% yield, 98.8% purity) as a white solid. LC-MS:  $R_t$  = 0.794 min,  $m/z$  = 302.1 (M + H)<sup>+</sup>;  $R_t$  = 0.787 min,  $m/z$  = 302.2 (M + H)<sup>+</sup>. HPLC:  $R_t$  = 2.682 min, purity: 98.8% under 220 nm. <sup>1</sup>H NMR: (400 MHz, MeOD)  $\delta$  7.24–7.20 (m, 2H), 7.14–7.12 (m, 3H), 3.60–3.51 (m, 2H), 2.74–2.63 (m, 3H), 2.30–2.28 (m, 2H), 2.20–2.18 (m, 2H), 1.94–1.84 (m, 6H), 1.45–1.42 (m, 1H), 1.32–1.24 (m, 4H). <sup>13</sup>C NMR: (400 MHz, MeOD)  $\delta$  174.65–174.39, 142.47–142.21, 129.76–129.36, 129.90, 70.57, 44.61–44.49, 43.73–43.46, 35.63, 34.97, 34.36, 33.24, 31.71, 30.65, 30.18.

**N-((1*r*,4*r*)-4-Hydroxycyclohexyl)-3-phenethylcyclopentane-1-carboxamide (9).** A mixture of dimethyl cyclopentane-1,3-dicarboxylate (**9a**, 2.00 g, 10.7 mmol, 1.00 equiv) and NaOH (429 mg, 10.7 mmol, 1.00 equiv) in MeOH (10.0 mL) was stirred for 12 h at 25 °C, filtered, and concentrated under reduced pressure to give a residue, purified by column chromatography to get 3-(methoxycarbonyl)cyclopentane-1-carboxylic acid (**9b**, 1.20 g, 6.97 mmol, 64.8% yield) as a light yellow oil. To a mixture of **9b** (1.10 g, 6.39 mmol, 1.00 equiv) in THF (10.0 mL) was added BH<sub>3</sub>-Me<sub>2</sub>S (10.0 M, 703  $\mu$ L, 1.10 equiv) at –78 °C, stirred for 0.5 h, then warmed to 25 °C, and stirred for 12 h to obtain methyl 3-(hydroxymethyl)cyclopentane-1-carboxylate (**9c**, 780 mg, 4.93 mmol, 77.1% yield) as a yellow oil. To a mixture of **9c** (780 mg, 4.93 mmol, 1.00 equiv) in DCM (10.0 mL) was added Dess–Martin (2.72 g, 6.41 mmol, 1.30 equiv) at 25 °C and was stirred for 2 h, dried over Na<sub>2</sub>SO<sub>4</sub>, filtered, and concentrated under reduced pressure to give a residue and was purified by column chromatography to obtain methyl 3-formylcyclopentane-1-carboxylate (**9d**, 283 mg, 1.81 mmol, 36.7% yield) as a light yellow oil. To a solution of benzyltriphenylphosphonium bromide (**9e**, 903 mg, 2.08 mmol, 1.15 equiv) in THF (10.0 mL) was added *t*-BuOK (329 mg, 2.94 mmol, 1.62 equiv) at –20 °C under N<sub>2</sub>, stirred for 1 h at –20 °C, and then added **9d** (183 mg, 1.81 mmol, 1.00 equiv) at –20 °C and stirred for another 1 h, filtered, and concentrated under reduced pressure to give a residue and was purified by column chromatography to get methyl (*E*)-3-styrylcyclopentane-1-carboxylate (124 mg, 538  $\mu$ mol, 29.7% yield) as a light yellow oil. To a solution of (*E*)-3-styrylcyclopentane-1-carboxylate (124 mg, 538  $\mu$ mol, 1.00 equiv) in MeOH (10.0 mL) was added Pd/C (120 mg, 10% purity) at 25 °C under H<sub>2</sub> (15 psi), stirred for 2 h at 25 °C to get methyl 3-phenethylcyclopentane-1-carboxylate (**9f**, 100 mg, 430  $\mu$ mol, 79.9% yield) as a light yellow oil. To a mixture of **9f** (85.0 mg, 365  $\mu$ mol, 1.00 equiv) in MeOH (5.00 mL), THF (5.00 mL), and H<sub>2</sub>O (2.00 mL) was added LiOH·H<sub>2</sub>O (30.7 mg, 731  $\mu$ mol, 2.00 equiv) at 25 °C; the mixture was heated to 70 °C and stirred for 2 h to get 3-phenethylcyclopentane-1-carboxylic acid (**9g**, 79.0 mg, 361  $\mu$ mol, 98.9% yield) as a light yellow oil. To a mixture of **9g** (79.0 mg, 361  $\mu$ mol, 1.00 equiv) and (*1*r*,4*r*)-4-aminocyclohexan-1-ol (65.8 mg, 434  $\mu$ mol, 1.20 equiv) in THF (10.0 mL) were added HATU (206 mg, 542  $\mu$ mol, 1.50 equiv) and Et<sub>3</sub>N (727 mg, 7.18 mmol, 1.00 mL) at 25 °C and stirred for 12 h. The reaction mixture was concentrated under reduced pressure to give a residue. The residue was purified by prep-HPLC (neutral condition, column: Waters Xbridge 150 mm  $\times$  25 mm  $\times$  5  $\mu$ m; mobile phase: [water (NH<sub>4</sub>HCO<sub>3</sub>)-ACN]; B%: 43–73%, 10 min). **9** (8.24 mg, 25.2  $\mu$ mol, 6.97% yield, 96.5% purity) was obtained as a white solid. LC-MS: RT = 0.933 min,  $m/z$  = 316.2 (M + H)<sup>+</sup>. HPLC: RT = 2.130 min, purity: 96.5% purity, under 220 nm. <sup>1</sup>H NMR: (400 MHz, DMSO-*d*<sub>6</sub>)  $\delta$  7.52 (d, *J* = 7.6, 1H), 7.27–7.23 (m, 2H), 7.18–7.15 (m, 3H), 4.52 (d, *J* = 4.0, 1H), 3.43–3.41 (m, 1H), 2.57–2.53 (m, 2H), 1.87–1.57 (m, 12H), 1.18–1.06 (m, 7H).*

**N-((1*r*,4*r*)-4-Hydroxycyclohexyl)-3-(3-phenylpropyl)cyclopentane-1-carboxamide (10).** To a solution of triphenyl(3-phenylpropyl)phosphonium bromide (**10b**, 1.79 g, 3.87 mmol, 1.10 equiv) in toluene (10.00 mL) was added *t*-BuOK (473 mg, 4.22 mmol, 1.20 equiv); the mixture was stirred at 70 °C for 1 h. Then, methyl 3-oxocyclopentane-1-carboxylate (**10a**, 500 mg, 3.52 mmol, 1.00 equiv) in toluene (2.00 mL) was added to the mixture and

stirred at 70 °C for 16 h to give methyl 3-(3-phenylpropylidene)cyclopentane-1-carboxylate (0.100 g, 388  $\mu$ mol, 11.0% yield, 94.8% purity) as a colorless oil; MeOH (10.0 mL) and Pd/C (0.10 g, 10% purity) were added at 25 °C and degassed with N<sub>2</sub> for 3 times. The resulting mixture was stirred at 25 °C under H<sub>2</sub> (15 psi) for 4 h; the mixture was filtered through celite, and the filtrate was concentrated under vacuum to give methyl 3-(3-phenylpropyl)cyclopentane-1-carboxylate (**10c**, 90.0 mg, 365  $\mu$ mol, 94.1% yield) as a colorless oil. A solution of **10c** (90.0 mg, 365  $\mu$ mol, 1.00 equiv) and LiOH·H<sub>2</sub>O (30.6 mg, 730  $\mu$ mol, 2.00 equiv) in MeOH (5.00 mL) and H<sub>2</sub>O (2.00 mL) was stirred at 70 °C for 3 h to obtain 3-(3-phenylpropyl)cyclopentane-1-carboxylic acid (**10d**, 90.0 mg, crude) as a yellow oil. A mixture of **10d** (90.0 mg, 387  $\mu$ mol, 1.00 equiv), (*1*r*,4*r*)-4-aminocyclohexan-1-ol (49.0 mg, 426  $\mu$ mol, 1.10 equiv), HATU (294 mg, 774  $\mu$ mol, 2.00 equiv), and Et<sub>3</sub>N (117 mg, 1.16 mmol, 161  $\mu$ L, 3.00 equiv) in THF (2.00 mL) was stirred at 25 °C for 16 h; the mixture was concentrated to give the residue and then purified by column: Phenomenex Gemini-NX C18 75 mm  $\times$  30 mm  $\times$  3  $\mu$ m; mobile phase: [water (0.225%FA)-ACN]; B%: 42–72%, 7 min. **11** (23.38 mg, 68.1  $\mu$ mol, 17.6% yield, 96.1% purity) was obtained as an off-white solid. LC-MS: RT = 0.859 min,  $m/z$  = 330.3 (M + H)<sup>+</sup>. HPLC: RT = 2.548 min, purity: 96.1%, under 220 nm. <sup>1</sup>H NMR: (400 MHz, DMSO-*d*<sub>6</sub>)  $\delta$  7.47 (d, *J* = 8.0, 1H), 7.28–7.24 (m, 2H), 7.18–7.15 (m, 3H), 4.49 (d, *J* = 4.0, 1H), 3.43–3.37 (m, 1H), 2.58–2.53 (m, 3H), 1.78–1.77 (m, 1H), 1.76–1.70 (m, 3H), 1.68–1.66 (m, 5H), 1.64–1.54 (m, 3H), 1.32–1.29 (m, 3H), 1.18–1.13 (m, 6H).*

**N-((1*r*,4*r*)-4-Hydroxycyclohexyl)-3-phenethylcyclohexane-1-carboxamide (11).** To a mixture of 3-(methoxycarbonyl)cyclohexane-1-carboxylic acid (**11a**, 2.00 g, 10.7 mmol, 1.00 equiv) in THF (10.0 mL) was added BH<sub>3</sub>-Me<sub>2</sub>S (10.0 M, 1.18 mL, 1.10 equiv) at –78 °C and stirred for 0.5 h at –78 °C and then warmed to 25 °C and stirred for 12 h to obtain methyl 3-(hydroxymethyl)cyclohexane-1-carboxylate (**11b**, 1.79 g, 10.4 mmol, 96.7% yield) as a light yellow oil. To a mixture of **11b** (1.79 g, 10.4 mmol, 1.00 equiv) and Et<sub>3</sub>N (6.31 g, 62.3 mmol, 6.00 equiv) in DMSO (20.0 mL) was added pyridine/sulfur trioxide (4.96 g, 31.2 mmol, 3.00 equiv) at 25 °C and stirred for 12 h, dried over Na<sub>2</sub>SO<sub>4</sub>, filtered, and concentrated under reduced pressure to give a residue. The residue was purified by column chromatography to get methyl 3-formylcyclohexane-1-carboxylate (**11c**, 710 mg, 4.17 mmol, 40.1% yield) as a yellow oil. To a solution of benzyltriphenylphosphonium bromide (1.17 g, 2.70 mmol, 1.15 equiv) in THF (10.0 mL) was added *t*-BuOK (427 mg, 3.81 mmol, 1.62 equiv) at –20 °C under N<sub>2</sub>, stirred for 1 h at –20 °C and then added **11c** (400 mg, 2.35 mmol, 1.00 equiv) at –20 °C and stirred for another 1 h. The product was dried over Na<sub>2</sub>SO<sub>4</sub>, filtered, and concentrated under reduced pressure to give a residue. The residue was purified by column chromatography to get intermediate methyl (*E*)-3-styrylcyclohexane-1-carboxylate (280 mg, 1.15 mmol, 48.7% yield) as a light yellow oil; then, MeOH (10.0 mL) and Pd/C (230 mg, 10% purity) were added at 25 °C under H<sub>2</sub> (15 psi) and stirred for 2 h to get methyl 3-phenethylcyclohexane-1-carboxylate (**11d**, 230 mg, 933  $\mu$ mol, 87.7% yield) as a colorless oil. To a mixture of **11d** (165 mg, 669  $\mu$ mol, 1.00 equiv) in MeOH (5.00 mL), THF (5.00 mL), and H<sub>2</sub>O (2.00 mL) was added LiOH·H<sub>2</sub>O (56.2 mg, 1.34  $\mu$ mol, 2.00 equiv) at 25 °C, then heated to 70 °C and stirred for 2 h to get 3-phenethylcyclohexane-1-carboxylic acid (**11e**, 150 mg, 645  $\mu$ mol, 96.4% yield) as a light yellow oil. To a mixture of **11e** (150 mg, 645  $\mu$ mol, 1.00 equiv) and (*1*r*,4*r*)-4-aminocyclohexan-1-ol (117 mg, 774  $\mu$ mol, 1.20 equiv) in THF (10.0 mL) were added HATU (368 mg, 968  $\mu$ mol, 1.50 equiv) and Et<sub>3</sub>N (1.45 g, 14.3 mmol, 2.00 mL) at 25 °C and stirred at 25 °C for 12 h. The reaction mixture was concentrated under reduced pressure to give a residue and was purified by prep-HPLC (neutral condition, column: Waters Xbridge 150 mm  $\times$  25 mm  $\times$  5  $\mu$ m; mobile phase: [water (NH<sub>4</sub>HCO<sub>3</sub>)-ACN]; B%: 40–70%, 10 min). **11** (8.15 mg, 24.3  $\mu$ mol, 3.78% yield, 98.6% purity) was obtained as a white solid. LC-MS: RT = 0.930 min,  $m/z$  = 330.2 (M + H)<sup>+</sup>. HPLC: RT = 2.218 min, purity: 98.6%, under 220 nm. <sup>1</sup>H NMR: (400 MHz, DMSO-*d*<sub>6</sub>)  $\delta$  7.46 (d, *J* = 8.0, 1H), 7.27–7.24 (m, 2H), 7.19–7.14 (m, 3H), 4.49 (s, 1H), 3.42–3.38 (m,*

1H), 2.59–2.55 (m, 2H), 2.04–1.98 (m, 1H), 1.79–1.69 (m, 8H), 1.58–1.40 (m, 4H), 1.24–1.11 (m, 6H), 1.09–0.96 (m, 1H), 0.90–0.77 (m, 1H).

***N*-((1*r*,4*r*)-4-Hydroxycyclohexyl)-4-phenethylcyclohexane-1-carboxamide (12).** A mixture of benzyltriphenylphosphonium bromide (1.47 g, 3.39 mmol, 1.15 equiv) and *t*-BuOK (535 mg, 4.77 mmol, 1.62 equiv) in THF (10.0 mL) was added at –20 °C under N<sub>2</sub> and was stirred for 1 h; then 4-formylcyclohexane-1-carboxylic acid (12a, 500 mg, 2.94 mmol, 1.00 equiv) was added at –20 °C and stirred for another 1 h, dried over Na<sub>2</sub>SO<sub>4</sub>, filtered, and concentrated under reduced pressure to give a residue and was purified by column chromatography to obtain an intermediate methyl (*E*)-4-styrylcyclohexane-1-carboxylate (130 mg, 530 μmol, 18.1% yield, 99.7% purity) as an off-white solid; then, MeOH (10.0 mL) and Pd/C (120 mg, 10% purity) were added at 25 °C under H<sub>2</sub> (15 psi), stirred for 2 h to get methyl 4-phenethylcyclohexane-1-carboxylate (12b, 120 mg, 487 μmol, 91.5% yield) as a light yellow oil. To a mixture of 12b (120 mg, 487 μmol, 1.00 equiv) in MeOH (5.00 mL), THF (5.00 mL), and H<sub>2</sub>O (2.00 mL) was added LiOH·H<sub>2</sub>O (40.9 mg, 974 μmol, 2.00 equiv) at 25 °C, then heated to 70 °C and stirred for 2 h to get 4-phenethylcyclohexane-1-carboxylic acid (12c, 110 mg, 473 μmol, 97.2% yield) as a light yellow oil; then, to a mixture of (1*r*,4*r*)-4-aminocyclohexan-1-ol (65.4 mg, 568 μmol, 1.20 equiv) in THF (10.0 mL) were added HATU (270 mg, 710 μmol, 1.50 equiv) and Et<sub>3</sub>N (143 mg, 1.42 mmol, 3.00 equiv) at 25 °C and stirred for 12 h. The reaction mixture was concentrated under reduced pressure to give a residue and was purified by prep-HPLC (neutral condition, column: Waters Xbridge 150 mm × 25 mm × 5 μm; mobile phase: [water (10 mM NH<sub>4</sub>HCO<sub>3</sub>)-ACN]; B%: 40–70%, 10 min). 12 (9.82 mg, 29.3 μmol, 6.21% yield, 98.6% purity) was obtained as a white solid. LC-MS: RT = 0.859 min, *m/z* = 330.3 (M + H)<sup>+</sup>. HPLC: RT = 2.236 min, purity: 98.6%, under 220 nm. <sup>1</sup>H NMR: (400 MHz, DMSO-*d*<sub>6</sub>) δ 7.45 (d, *J* = 8.0, 1H), 7.27–7.24 (m, 2H), 7.18–7.15 (m, 3H), 4.48 (d, *J* = 4.0, 1H), 3.46–3.36 (m, 2H), 2.59–2.55 (m, 2H), 2.03–1.96 (m, 1H), 1.80–1.76 (m, 4H), 1.69–1.64 (m, 4H), 1.45–1.43 (m, 2H), 1.35–1.25 (m, 2H), 1.25–1.13 (m, 5H), 0.91–0.87 (m, 2H).

**4-Benzyl-*N*-((1*r*,4*r*)-4-hydroxycyclohexyl)cyclohexane-1-carboxamide (13).** A mixture of methyl 4-(4,4,5,5-tetramethyl-1,3,2-dioxaborolan-2-yl)cyclohex-3-ene-1-carboxylate (13a, 500 mg, 1.88 mmol, 1.15 equiv) and (bromomethyl)benzene (385 mg, 2.25 mmol, 1.20 equiv) in dioxane (10.0 mL) and H<sub>2</sub>O (2.00 mL) were added Pd(dppf)Cl<sub>2</sub> (274 mg, 375 μmol, 0.20 equiv) and K<sub>2</sub>CO<sub>3</sub> (778 mg, 5.64 mmol, 3.00 equiv) at 25 °C under N<sub>2</sub>. The mixture was heated to 100 °C and stirred for 2 h to get intermediate methyl 4-benzylcyclohex-3-ene-1-carboxylate (300 mg, 1.30 mmol, 69.3% yield) as a light yellow oil. To a solution of the intermediate (300 mg, 1.30 mmol, 1.00 equiv) in MeOH (10.0 mL) was added Pd/C (300 mg, 10% purity) at 25 °C under H<sub>2</sub> (15 psi) and was stirred for 2 h at 25 °C to obtain methyl 4-benzylcyclohexane-1-carboxylate (13b, 300 mg, 1.29 mmol, 99.1% yield) as a light yellow oil. To a mixture of 13b (300 mg, 1.29 mmol, 1.00 equiv) in MeOH (5.00 mL), THF (5.00 mL), and H<sub>2</sub>O (2.00 mL) was added LiOH·H<sub>2</sub>O (108 mg, 2.58 mmol, 2.00 equiv) at 25 °C and then heated to 70 °C and stirred for 2 h to get 4-benzylcyclohexane-1-carboxylic acid (13c, 280 mg, 1.28 mmol, 99.3% yield) as a light yellow oil. To a mixture of 13c (280 mg, 1.28 mmol, 1.00 equiv) and (1*r*,4*r*)-4-aminocyclohexan-1-ol (147 mg, 1.28 mmol, 1.00 equiv) in THF (5.00 mL) were added HATU (731 mg, 1.92 mmol, 1.50 equiv) and Et<sub>3</sub>N (389 mg, 3.85 mmol, 3.00 equiv) at 25 °C and stirred for 12 h. The reaction mixture was concentrated under reduced pressure to give a residue. The residue was purified by prep-HPLC (neutral condition, column: Waters Xbridge 150 mm × 25 mm × 5 μm; mobile phase: [water (10 mM NH<sub>4</sub>HCO<sub>3</sub>)-ACN]; B%: 37–67%, 10 min). 13 (58.93 mg, 185 μmol, 14.4% yield, 99.0% purity) was obtained as a white solid. LC-MS: RT = 0.823 min, *m/z* = 316.3 (M + H)<sup>+</sup>. HPLC: RT = 2.097 min, purity: 99.0%, under 220 nm. <sup>1</sup>H NMR: (400 MHz, CDCl<sub>3</sub>-*d*<sub>1</sub>) δ 7.21–7.17 (m, 2H), 7.11–7.05 (m, 3H), 5.24 (d, *J* = 7.6, 1H), 3.72–3.68 (m, 1H), 3.54–3.51 (m, 1H), 2.52 (d, *J* = 7.6, 2H), 2.15–2.13 (m, 1H), 1.93–1.91 (m, 4H), 1.84–1.66 (m, 4H), 1.46–1.36 (m, 7H), 1.12–1.09 (m, 2H).

**2-((Benzylthio)methyl)-*N*-((1*r*,4*r*)-4-hydroxycyclohexyl)cyclopropane-1-carboxamide (14, 14A, and 14B).** Phenylmethanethiol (14a, 25.2 g, 202 mmol, 23.7 mL, 1.00 equiv) was added to a solution of EtONa (13.8 g, 202 mmol, 1.00 equiv) in EtOH (100 mL), KI (1.68 g, 10.1 mmol, 0.05 equiv), and 2-chloro-1,1-dimethoxyethane (30.3 g, 243 mmol, 27.8 mL, 1.20 equiv); the mixture was stirred at 80 °C for 12 h; the reaction mixture was filtered, concentrated under reduced pressure, and purified by flash silica gel chromatography to obtain benzyl(2,2-dimethoxyethyl)sulfane (38.0 g, 179 mmol, 88.2% yield). H<sub>2</sub>SO<sub>4</sub> (17.9 g, 179 mmol, 9.74 mL, 98.0% purity, 1.00 equiv) was added and stirred at 60 °C for 12 h to obtain 2-(benzylthio)acetaldehyde (14b, 27.0 g). *tert*-Butyl 2-(triphenyl-λ<sup>5</sup>-phosphanyliden)acetate (64.7 g, 172 mmol, 1.30 equiv) was added to a solution of 14b (22.0 g, 132 mmol, 1.00 equiv) in THF (220 mL) and stirred at 20 °C for 12 h to obtain *tert*-butyl (*E*)-4-(benzylthio)but-2-enoate (14c, 31.3 g). To a solution of NaH (3.87 g, 96.6 mmol, 60.0% purity, 1.20 equiv) in DMSO (100 mL) was added dimethylmethanesulfinic iodide (21.2 g, 96.6 mmol, 1.20 equiv), and the mixture was stirred at 20 °C for 0.5 h, then added a solution of 14c (21.3 g, 80.5 mmol, 1.00 equiv) and stirred at 20 °C for 1 h to obtain *tert*-butyl 2-((benzylthio)methyl)cyclopropane-1-carboxylate (14d, 4.10 g, 14.7 mmol, 18.2% yield). To a solution of 14d (4.10 g, 14.7 mmol, 1.00 equiv) in DCM (20.0 mL) was added TFA (36.1 g, 316 mmol, 23.4 mL, 21.5 equiv); the mixture was stirred at 25 °C for 16 h to obtain 2-((benzylthio)methyl)cyclopropane-1-carboxylic acid (14e, 2.30 g). To a solution of 14e (2.30 g, 10.3 mmol, 1.00 equiv) in DMF (20.0 mL) were added EDCI (2.98 g, 15.5 mmol, 1.50 equiv), HOBt (1.68 g, 12.4 mmol, 1.20 equiv), and DIEA (2.68 g, 20.7 mmol, 3.61 mL, 2.00 equiv). Then, (1*r*,4*r*)-4-aminocyclohexan-1-ol (1.73 g, 11.3 mmol, 1.10 equiv) was added to the mixture and stirred at 25 °C for 2 h. The reaction mixture was poured into water (90.0 mL), stirred at 25 °C for 1 h, filtered, and the filtrate was evaporated under vacuum; the product was triturated with ethyl acetate (30.0 mL) at 70 °C for 30 min, then cooled to 25 °C, filtered, and the filtrate was concentrated under vacuum; the residue was purified by prep-HPLC (column: Phenomenex luna C18 250 mm × 50 mm × 10 μm; mobile phase: [water (0.1%TFA)-ACN]; B%: 20–50%, 20 min). To get the individual enantiomers 14A and 14B, the product was purified by prep-SFC (column: DAICEL CHIRALPAK AD-H (250 mm × 30 mm, 5 μm); mobile phase: [0.1% NH<sub>3</sub>H<sub>2</sub>O EtOH]; B%: 35–35%, 2.7 min; 240 min). The product was purified by (column: Phenomenex Gemini-NX C18 75 mm × 30 mm × 3 μm; mobile phase: [water (0.05% ammonia hydroxide v/v)-ACN]; B%: 15–45%, 7 min) and (column: Phenomenex Gemini-NX C18 75 mm × 30 mm × 3 μm; mobile phase: [water (0.225%FA)-ACN]; B%: 30–60%, 2 min). 14A (1.37 g, 4.22 mmol, 40.7% yield, 98.4% purity) was obtained as an off-white solid and 14B (1.18 g, 3.59 mmol, 34.7% yield, 97.3% purity) was obtained as an off-white solid. LC-MS: 14A: RT = 0.816 min, *m/z* = 320.2 (M + H)<sup>+</sup>; 14B: RT = 0.645 min, *m/z* = 319.9 (M + H)<sup>+</sup>. HPLC: 14A: RT = 1.887 min, purity: 98.4%, under 220 nm. 14B: RT = 1.880 min, purity: 97.3%, under 220 nm. <sup>1</sup>H NMR: 14A: (400 MHz MeOD) δ 7.33–7.21 (m, 5H), 3.76 (s, 2H), 3.60–3.57 (m, 1H), 3.52–3.50 (m, 1H), 2.44–2.40 (m, 2H), 1.94–1.89 (m, 4H), 1.42–1.40 (m, 2H), 1.33–1.29 (m, 4H), 1.08 (td, *J* = 4.4, 8.8 Hz, 1H), 0.69 (ddd, *J* = 4.2, 6.0, 8.4 Hz, 1H); 14B: (400 MHz MeOD) δ 7.32–7.28 (m, 5H), 3.76 (s, 2H), 3.61–3.58 (m, 1H), 3.52–3.50 (m, 1H), 2.44–2.40 (m, 2H), 1.94–1.89 (m, 4H), 1.43–1.41 (m, 2H), 1.33–1.28 (m, 4H), 1.08 (td, *J* = 4.4, 8.8 Hz, 1H), 0.69 (ddd, *J* = 4.2, 6.0, 8.4 Hz, 1H).

**X-ray Diffraction Studies of 14A and 14B.** X-ray Powder Diffraction (XRPD). Studies were performed with a Panalytical X'Pert3 Powder XRPD on a Si zero-background holder. The 2θ position was calibrated against a Panalytical Si reference standard disc. The parameters used are shown in Table S2.

**TGA/DSC Thermogravimetric Analysis (TGA).** Data were collected using a TA Discovery 550 TGA from TA Instrument. Differential scanning calorimetry (DSC) was performed using a TA 2500 DSC from TA Instrument. DSC was calibrated with the indium reference

standard, and the TGA was calibrated using the nickel reference standard. Detailed parameters used are shown in Table S3.

**Polarized Light Microscopy.** Crystal images were captured on a Nikon DS-Fi2 upright microscope at room temperature.

**Single-Crystal Data Collection.** The X-ray intensity data were measured on a Bruker D8 VENTURE ( $\mu$ S microfocus X-ray source, Cu K $\alpha$ ,  $\lambda = 1.54178$  Å, PHOTON CMOS detector) diffractometer. The strategy was created and optimized with Bruker Apex3 software, and the frames were integrated with the Bruker SAINT software package. Data were corrected for absorption effects using the multiscan method (SADABS-2016/2). The structure was solved with the ShelXT structure solution program using intrinsic phasing and refined with the ShelXL (Version 2014/7) refinement package using full-matrix least-squares on  $F^2$  contained in the SHELX software suite.<sup>24,25</sup>

**Single-Crystal Growth Experiments. Slow Evaporation.** HPLC vials with saturated solutions of **14A** and **14B** were capped with perforated caps. Vials were left at RT to allow slow evaporation of the solvents. A total of 20 experiments were prepared, of which 4 are represented in Table S4. The remaining 16 samples were moved to slow cooling due to limited observed solubility. The summary of slow evaporation experiments is shown in Table S4.

Layer diffusion was performed in HPLC vials with saturated solutions of **14A** and **14B**. Antisolvents were layered onto the saturated solutions slowly and the vial was capped. Vials were left at room temperature to allow the two solvents to diffuse into one another. A total of 20 experiments were performed, with results shown below. The summary of layer diffusion experiments is shown in Table S5.

**Slow Cooling.** Saturated solutions of **14A** and **14B** were prepared by slurrying at 35–60 °C in HPLC vials. Suspensions were filtered using a PTFE membrane (pore size 0.20  $\mu$ m). Filtrates were slowly cooled to 5 °C at a rate of 0.1 °C/min. A total of 15 experiments were performed; the results are shown in Table S1.

**Dose–Response of Mitofusin Agonist Fusogenicity.** The dose–response was measured using a mitochondrial elongation assay (aspect ratio) performed in Mfn1- or Mfn2-deficient MEFs cultured at 37 °C, 5% CO<sub>2</sub>–95% air; cells were seeded on day 1 in 6-well plates at a density of  $2 \times 10^4$  cells/well, and compounds were added at nine concentrations (0.5 nM to 10  $\mu$ M dissolved in DMSO) overnight. Mitochondria were then stained with MitoTracker Orange (200 nM; M7510; Invitrogen, Carlsbad, CA), and nuclei were stained with Hoechst (10  $\mu$ g/mL; Invitrogen, Thermo Fisher Scientific Cat: # H3570). Images were acquired at room temperature on a Nikon Ti confocal microscope using a 60  $\times$  1.3 NA oil-immersion objective in the Krebs–Henseleit buffer (138 NaCl, 3.7 nM KCL, 1.2 nM KH<sub>2</sub>PO<sub>4</sub>, 15 nM glucose, 20 nM HEPES pH: 7.2–7.5, and 1 mM CaCl<sub>2</sub>). Laser excitation was 549 nm with an emission at 590 nm for MitoTracker Orange and the excitation was 306 nm with an emission at 405 nm for Hoechst. Images were analyzed using ImageJ and fusogenicity was quantified as the mitochondrial aspect ratio (length/width) and were indexed to the maximal response elicited by 1. Response curves were interpolated by the sigmoidal model using Prism 8 software. EC<sub>50</sub> values are reported as mean with 95% confidence limits for at least three independent experiments.<sup>16</sup>

**Functional Evaluation of Mitofusin Agonist Effect on Mitochondrial Depolarization.** Cultured Mfn2 KO or Mfn1 KO MEFs were treated with either DMSO, **1**, **5A**, or **5B** (1  $\mu$ M) for 48 h and then stained with tetramethylrhodamine ethyl ester (TMRE, 200 nM, Invitrogen Thermo Fisher Scientific Cat:# T-669), MitoTracker Green (200 nM; Invitrogen, Thermo Fisher Scientific Cat:# M7514) and Hoechst (10  $\mu$ g/mL; Invitrogen, Thermo Fisher Scientific Cat:# H3570) were added for 30 min at 37 °C in 5% CO<sub>2</sub>–95% air, and washed twice in PBS. Images were acquired at room temperature on a Nikon Ti confocal microscope using either 60  $\times$  1.3 NA oil-immersion objective in the Krebs–Henseleit buffer (138 NaCl, 3.7 nM KCL, 1.2 nM KH<sub>2</sub>PO<sub>4</sub>, 15 nM glucose, 20 nM HEPES pH: 7.2–7.5, and 1 mM CaCl<sub>2</sub>): laser excitation was 488 nm with emission at 510 nm for MitoTracker Green, 549 nm with emission at 590 nm for TMRE, and 306 nm with emission 405 nm for Hoechst.

Mitochondrial depolarization was reported as the % number of green mitochondria/number of yellow+green mitochondria using ImageJ.<sup>16</sup>

**FRET studies of MFN2 conformation** were performed as previously described.<sup>15,16</sup> Briefly, the MFN2 FRET protein engineered with amino terminal mCerulean and carboxy terminal mVenus reporters<sup>14</sup> was expressed with an adenoviral vector in mitofusin null (MFN1/MFN2 knockout) MEFs cultured in UV transparent 96-well plates. Forty-eight hours thereafter, 1  $\mu$ M of each test compound or vehicle (DMSO) was added for 4 h. Fluorescence signals were acquired on a Tecan Safire II multimode plate reader: FRET-excitation 433/8 nm, emission 528/8 nm; cerulean-excitation 433/8 nm, emission 475/8 nm.

Mitofusin agonist pharmacodynamic effects on the sciatic nerve motility were measured using time-lapse imaging (1 frame every 5 s) for 121 frames (10 min, sciatic nerve) at 37 °C on a Nikon A1Rsi confocal microscope using a 40x oil objective as described. Sciatic nerve axon mitochondria were labeled with TMRE. Kymographs and quantitative data were generated using an ImageJ plug-in.<sup>17</sup>

*In vitro* pharmacokinetic analyses of mitofusin agonists were performed in duplicate using standard methods by WuXi Apptec Co. Ltd. (Shanghai, China). Plasma protein binding was measured by equilibrium dialysis; % bound =  $(1 - [\text{free compound in dialysate}] / [\text{total compound in retentate}]) \times 100$ . Plasma stability of 2  $\mu$ M compounds in clarified freeze–thawed plasma was assessed by LC-MS/MS of supernatants after protein precipitation; 120 min data are reported for studies including 0, 10, 30, 60, and 120 min. Liver microsome stability of 1  $\mu$ M compounds was studied in liver microsomes (0.5 mg/mL) after 0, 5, 10, 20, 30, and 60 min. Incubation was assessed by LC/MS/MS of reaction extracts. Passive artificial blood–brain barrier membrane permeability assay (PAMPA-BBB) was performed using 150  $\mu$ L of 10  $\mu$ M compounds (5% DMSO) added to PVDF membranes precoated with 5  $\mu$ L of 1% brain polar lipid extract (Porcine)/dodecane mixture and incubated for 4 h at room temperature with shaking at 300 rpm. Donor and acceptor samples were analyzed by LC-MS/MS.

*In vivo* pharmacokinetic analyses were performed in triplicate at WuXi Apptec Co. Ltd. (Shanghai, China) or Frontage Laboratories, Inc. (Exton, PA). Except where specifically noted, compounds were administered orally to mice fasted overnight, with food returned 4 h post dosing. Compounds **2** and **5B** (5 mg/mL) were dissolved in 30% SBE- $\beta$ -CD and administered by oral gavage (50 mg/kg) to 7–9 week male CD-1 mice; plasma was collected and brains were prepared by homogenizing with 4 vol (w/v) of the homogenizing solution (MeOH/15 mM PBS (1:2, v/v)) followed by further diluting in the blank matrix to obtain dilution factors of 40 and 10. A 40  $\mu$ L aliquot of the study sample was quenched with 800  $\mu$ L of IS1 (6 in 1 internal standard in ACN (Labetalol & tolbutamide & Verapamil & dexamethasone & glyburide & Celecoxib 100 ng/mL for each)), respectively, and then the mixture was vortex-mixed well (at least 15 s) and centrifuged for 15 min at 12 000g, 4 °C; an aliquot of 60  $\mu$ L supernatant was transferred to a 96-well plate and centrifuged for 5 min at 3220g, 4 °C; then, the supernatant was directly injected for HPLC analysis. Compound **5** enantiomeric mixture was dissolved in 10% DMSO/90% (30% HP- $\beta$ -CD) and administered intravenously (10 mg/kg) or **5B** (5 mg/mL) was dissolved in 10% DMSO/90% (30% HP- $\beta$ -CD) and administered by oral gavage (50 mg/kg) to 7–9 week male CD-1 mice. Plasma was collected; the brain, nerve, and spinal cord samples were homogenized in water with 4, 8, and 4 dilution factors, respectively. Plasma, spinal cord, and nerve homogenates were further diluted in control mouse plasma to achieve a total dilution factor of 10, 20, and 40, respectively. For mouse study samples, 30  $\mu$ L of each sample was added to separate wells of the 96-well plate and 30  $\mu$ L of diluent (ACN/H<sub>2</sub>O, 50:50) was added to each sample. To all samples, 200  $\mu$ L of internal standard (200 ng/mL warfarin) solution in ACN was added. The plate was vortexed vigorously for 10 min and then centrifuged for 10 min at 4000 rpm (Sorvall Legend X1R centrifuge, Thermo Scientific) at 15 °C. Supernatants were further diluted 1:1 in H<sub>2</sub>O prior to HPLC analysis. Time–concentration curves were generated using noncompartmental

approaches and Phoenix WinNonlin 6.3 software. Data are presented as mean  $\pm$  SEM from three mice for each condition.

**Measuring Effects of 2 and 5 on Neuromuscular Dysfunction in Murine ALS.** ALS (SOD1G93A) mice<sup>24</sup> were randomly assigned to oral treatment with vehicle (10% Me<sub>2</sub>SO/90%, 30% 2-hydroxypropyl- $\beta$ -cyclodextrin) (HP-BCD; Sigma-Aldrich, Cat:# 332607) or 5 (60 mg/kg twice daily) from age 60 through 140 days. Disease severity was assessed by investigators blind to treatment status using an integrated multitest scoring system<sup>25</sup> as follows.

**Ledge Test.** Score 0 = effectively uses its hind legs while walking along the ledge of the cage; score 1 = loses its footing some times while walking along the ledge but appears coordinated; score 2 = it does not effectively use its hind legs; and score 3 = refuses to move along the ledge or falls off from the ledge while walking.

**Hindlimb Clasp.** Score 0 = hindlimbs are completely splayed outward while being lifted by grasping its tail; score 1 = one hindlimb is partially collapsed toward the abdomen; score 2 = both hindlimbs are partially collapsed toward the abdomen; and score 3 = hindlimbs are entirely touching the abdomen.

**Gait.** Score 0 = it appears normal gait when the mice are allowed to walk; score 1 = it is tremor or appears to limp while walking; score 2 = feet pointed away from the body while walking; and score 3 = it has difficulty moving forward.

**Kyphosis.** Score 0 = it is able to straighten its spine while walking, and no kyphosis is observed; score 1 = it shows mild kyphosis but is able to straighten its spine; score 2 = it is unable to straighten its spine but mild kyphosis; and score 3 = severe kyphosis while walking and sitting.

The aggregate dysfunction score as reported is the sum of all four individual test scores.

**Lipinski's Rule and Central Nervous System Multiparameter Optimization Calculation.** Lipinski's rule-related compound properties were calculated using DruLiTo software. Chemical properties of compounds were obtained using ACD/Laboratories, version 12.1, for ClogD at pH 7.4, pK<sub>a</sub>. For calculation of TPSA, clogP was obtained using Chemdraw 19.1. The CNS MPO scores were calculated as described.<sup>29–31</sup>

**PAINS Analysis.** All reported compounds were screened for PAINS through the FAF-Drugs4 website tool (<https://mobyli.rpbs.univ-paris-diderot.fr/cgi-bin/portal.py#welcome>), and none were identified as pan assay interference compounds.

**Animals.** ALS B6.SOD1G93A mice<sup>24</sup> were purchased from The Jackson Laboratory (Stock No. 004435). Mouse procedures were approved by the Institutional Animal Care and Use Committee of Washington University in St. Louis Protocol ID: 19-0910, by IACUC-SH for the WuXi Corporate Committee for Animal Research Ethics, by the Confluence Discovery Technologies Animal Care and Use Committee, and by the Frontage Labs Animal Care and Use Committee.

## ■ ASSOCIATED CONTENT

### SI Supporting Information

The Supporting Information is available free of charge at <https://pubs.acs.org/doi/10.1021/acs.jmedchem.1c00163>.

Dose–response curves and EC<sub>50</sub> values of 1–6 (Figure S1); <sup>1</sup>H NMR spectrum of intermediate 5C (Figure S2); characteristics of 9 and 10 starting materials (Figure S3); crystallization of 9 and 10 for single-crystal X-ray diffraction studies (Figure S4); structural modeling of positions for human MFN2 amino acids mimicked by small molecule mitofusin activators (Figure S5); HPLC, <sup>1</sup>H NMR, and <sup>13</sup>C NMR chromatographies of 5 (Figure S6); HPLC, <sup>1</sup>H NMR, and <sup>13</sup>C NMR chromatographies of 6 (Figure S7); HPLC, <sup>1</sup>H NMR, and <sup>13</sup>C NMR chromatographies of 7 (Figure S8); HPLC, <sup>1</sup>H NMR, and <sup>13</sup>C NMR chromatographies of 8 (Figure S9); HPLC and <sup>1</sup>H NMR chromatography of 9 (Figure S10);

HPLC and <sup>1</sup>H NMR chromatography of 10 (Figure S11); HPLC and <sup>1</sup>H NMR chromatography of 11 (Figure S12); HPLC and <sup>1</sup>H NMR chromatography of 12 (Figure S13); HPLC and <sup>1</sup>H NMR chromatography of 13 (Figure S14); SFC, <sup>1</sup>H NMR, and <sup>13</sup>C NMR chromatographies of 5A and 5B (Figure S15); HPLC and <sup>1</sup>H NMR chromatography of 14A and 14B (Figure S16); solvents used in slow cooling experiments (Table S1); parameters used in X-ray powder diffraction (Table S2); parameters used in thermogravimetric analysis (TGA) and differential scanning calorimetry (DSC) (Table S3); summary of slow evaporation experiments (Table S4); and summary of layer diffusion experiments (Table S5) (PDF)

hMFN2 wt (PDB)

6jfm (PDB)

Molecular formula string for all of the final compounds (CSV)

## ■ Accession Codes

CCDC 2057833–2057834 contains the supplementary crystallographic data for this paper. These data can be obtained free of charge via [www.ccdc.cam.ac.uk/data\\_request/cif](http://www.ccdc.cam.ac.uk/data_request/cif), or by emailing [data\\_request@ccdc.cam.ac.uk](mailto:data_request@ccdc.cam.ac.uk), or by contacting The Cambridge Crystallographic Data Centre, 12 Union Road, Cambridge CB2 1EZ, UK; fax: +44 1223 336033.

## ■ AUTHOR INFORMATION

### Corresponding Author

Gerald W. Dorn, II – Department of Internal Medicine, Washington University School of Medicine, St. Louis, Missouri 63110, United States; Mitochondria in Motion, Inc., St. Louis, Missouri 63110, United States; Phone: 314 362-4892; Email: [gdorn@wustl.edu](mailto:gdorn@wustl.edu); Fax: 314 362-8844

### Authors

Xiawei Dang – Department of Cardiology, The First Affiliated Hospital of Xi'an Jiao Tong University, Xi'an, Shaanxi 710061, China; Department of Internal Medicine, Washington University School of Medicine, St. Louis, Missouri 63110, United States; [orcid.org/0000-0002-0343-7107](https://orcid.org/0000-0002-0343-7107)

Sidney B. Williams – Mitochondria in Motion, Inc., St. Louis, Missouri 63110, United States

Sriram Devanathan – Mitochondria in Motion, Inc., St. Louis, Missouri 63110, United States

Antonietta Franco – Department of Internal Medicine, Washington University School of Medicine, St. Louis, Missouri 63110, United States

Lijun Fu – WuXi AppTec Co., Ltd., Wuhan, Hubei 430075, China

Peter R. Bernstein – PharmaB LLC, Philadelphia, Pennsylvania 19102, United States; [orcid.org/0000-0003-0407-9150](https://orcid.org/0000-0003-0407-9150)

Daniel Walters – Crystal Pharmatech Inc., Cranbury, New Jersey 08512, United States

Complete contact information is available at:

<https://pubs.acs.org/doi/10.1021/acs.jmedchem.1c00163>

### Author Contributions

G.W.D. conceived of the compounds and designed the research. G.W.D., X.D., L.F., P.R.B., and D.W. wrote the

manuscript. S.W. performed *in vivo* pharmacokinetic studies for 5B. X.D. performed all mitochondria studies. X.D. and A.F. performed FRET studies. L.F. synthesized compounds. D.W. performed XRD studies. S.D. and P.R.B. provided input into compound analyses.

### Funding

X.D. was supported, in part, by the China Scholarship Council and G.W.D. by NIH R41NS113642, R41NS115184, R35135736, and Research Grant 628906 from the Muscular Dystrophy Association. G.W.D. is the Philip and Sima K. Needleman-endowed Professor at Washington University in St. Louis and a Scholar-Innovator awardee of the Harrington Discovery Institute.

### Notes

The authors declare the following competing financial interest(s): G.W.D. is an inventor on patent applications PCT/US18/028514 submitted by Washington University and PCT/US19/46356 and PCT/US20/14784 submitted by Mitochondria Emotion, Inc., that cover the use of small molecule mitofusin agonists to treat chronic neurodegenerative diseases and is the founder of Mitochondria in Motion, Inc., a SaintLouis-based biotech R&D company focused on enhancing mitochondrial trafficking and fitness in neurodegenerative diseases. The other authors declare no competing interests. Studies were performed under terms of an MTA between mitochondria in Motion, Inc., and Washington University in St. Louis.

Human Mfn1 (PDB ID: 5GNS) and Arabidopsis thaliana dynamin-related protein (PDB ID: 3T34) were used to computationally model human Mfn2 closed configuration based on structural homology, which has been described previously.<sup>15</sup> And this hypothetical human Mfn2 structure and hMFN2 found in the protein database (PDB; code 6JFM) were used for molecular modeling with compounds 14A and 14B; the authors will release the atomic coordinates and experimental data upon article publication.

### ACKNOWLEDGMENTS

We are very grateful for Yanchun Lin for helping us with the synthetic schemes.

### ABBREVIATIONS USED

ACN, acetonitrile; ALS, amyotrophic lateral sclerosis; CDI, 1,1'-carbonyldiimidazole; CMT2A, Charcot–Marie–Tooth disease type 2A; DCC, N,N'-dicyclohexylcarbodiimide; DCM, dichloromethane; DEAD, diethyl azodicarboxylate; DIPEA, N,N-diisopropylethylamine; DMF, dimethylformamide; DMSO, dimethyl sulfoxide; EDCl, N-ethyl-N'-(3-dimethylaminopropyl)carbodiimide hydrochloride; EtOAc, ethyl acetate; EtOH, ethanol; FRET, Förster resonance energy transfer; HP-*b*-CD, 2-hydroxypropyl- $\beta$ -cyclodextrin; HPLC, high-performance liquid chromatography; HRMS, high-resolution mass spectrometry; PA, isopropyl alcohol; IMIBK, 4-methyl-2-pentanone; IPAc, isopropyl acetate; LC-MS, liquid chromatography tandem mass spectrometry; MEFs, mouse embryonic fibroblasts; MEK, methyl ethyl ketone; MeOH, methanol; 2-MeTHF, 2-methyltetrahydrofuran; MFN, mitofusin; MTBE, methyl *tert*-butyl ether; NMR, nuclear magnetic resonance; PAMPA-BBB, passive artificial blood–brain barrier membrane permeability assay; PBS, phosphate-buffered saline; PK, pharmacokinetic; PPH3, triphenylphosphine; r.t., room temperature; SFC, supercritical fluid chromatography; TEA,

triethylamine; THF, tetrahydrofuran; tPSA, topological polar surface area

### REFERENCES

- (1) Knott, A. B.; Perkins, G.; Schwarzenbacher, R.; Bossy-Wetzel, E. Mitochondrial fragmentation in neurodegeneration. *Nat. Rev. Neurosci.* **2008**, *9*, 505–518.
- (2) Chan, D. C. Fusion and fission: Interlinked processes critical for mitochondrial health. *Annu. Rev. Genet.* **2012**, *46*, 265–287.
- (3) Koshiba, T.; Detmer, S. A.; Kaiser, J. T.; Chen, H.; McCaffery, J. M.; Chan, D. C. Structural basis of mitochondrial tethering by mitofusin complexes. *Science* **2004**, *305*, 858–862.
- (4) Chen, H.; Detmer, S. A.; Ewald, A. J.; Griffin, E. E.; Fraser, S. E.; Chan, D. C. Mitofusins mfn1 and mfn2 coordinately regulate mitochondrial fusion and are essential for embryonic development. *J. Cell Biol.* **2003**, *160*, 189–200.
- (5) Eura, Y.; Ishihara, N.; Yokota, S.; Mihara, K. Two mitofusin proteins, mammalian homologues of fzo, with distinct functions are both required for mitochondrial fusion. *J. Biochem.* **2003**, *134*, 333–344.
- (6) Dorn, G. W., II Evolving concepts of mitochondrial dynamics. *Annu. Rev. Physiol.* **2019**, *81*, 1–17.
- (7) Feely, S. M.; Laura, M.; Siskind, C. E.; Sottile, S.; Davis, M.; Gibbons, V. S.; Reilly, M. M.; Shy, M. E. Mfn2 mutations cause severe phenotypes in most patients with cmt2a. *Neurology* **2011**, *76*, 1690–1696.
- (8) Stuppia, G.; Rizzo, F.; Riboldi, G.; Del Bo, R.; Nizzardo, M.; Simone, C.; Comi, G. P.; Bresolin, N.; Corti, S. Mfn2-related neuropathies: Clinical features, molecular pathogenesis and therapeutic perspectives. *J. Neurol. Sci.* **2015**, *356*, 7–18.
- (9) Wang, L.; Gao, J.; Liu, J.; Siedlak, S. L.; Torres, S.; Fujioka, H.; Huntley, M. L.; Jiang, Y.; Ji, H.; Yan, T.; Harland, M.; Termsarasab, P.; Zeng, S.; Jiang, Z.; Liang, J.; Perry, G.; Hoppel, C.; Zhang, C.; Li, H.; Wang, X. Mitofusin 2 regulates axonal transport of calpastatin to prevent neuromuscular synaptic elimination in skeletal muscles. *Cell Metab.* **2018**, *28*, 400–414.e408.
- (10) Kim, J.; Moody, J. P.; Edgerly, C. K.; Bordiuk, O. L.; Cormier, K.; Smith, K.; Beal, M. F.; Ferrante, R. J. Mitochondrial loss, dysfunction and altered dynamics in huntington's disease. *Hum. Mol. Genet.* **2010**, *19*, 3919–3935.
- (11) Zorzano, A.; Sebastian, D.; Segales, J.; Palacin, M. The molecular machinery of mitochondrial fusion and fission: An opportunity for drug discovery? *Curr. Opin. Drug Discovery Dev.* **2009**, *12*, 597–606.
- (12) Miret-Casals, L.; Sebastián, D.; Brea, J.; Rico-Leo, E. M.; Palacin, M.; Fernández-Salguero, P. M.; Loza, M. I.; Albericio, F.; Zorzano, A. Identification of new activators of mitochondrial fusion reveals a link between mitochondrial morphology and pyrimidine metabolism. *Cell Chem. Biol.* **2018**, *25*, 268–278.e264.
- (13) Wang, D.; Wang, J.; Bonamy, G. M.; Meeusen, S.; Brusch, R. G.; Turk, C.; Yang, P.; Schultz, P. G. A small molecule promotes mitochondrial fusion in mammalian cells. *Angew. Chem., Int. Ed.* **2012**, *51*, 9302–9305.
- (14) Franco, A.; Kitsis, R. N.; Fleischer, J. A.; Gavathiotis, E.; Kornfeld, O. S.; Gong, G.; Biris, N.; Benz, A.; Qyit, N.; Donnelly, S. K.; Chen, Y.; Mennerick, S.; Hodgson, L.; Mochly-Rosen, D.; Dorn, G. W., II. Correcting mitochondrial fusion by manipulating mitofusin conformations. *Nature* **2016**, *540*, 74–79.
- (15) Rocha, A. G.; Franco, A.; Krezel, A. M.; Rumsey, J. M.; Alberti, J. M.; Knight, W. C.; Biris, N.; Zacharioudakis, E.; Janetka, J. W.; Baloh, R. H.; Kitsis, R. N.; Mochly-Rosen, D.; Townsend, R. R.; Gavathiotis, E.; Dorn, G. W., II Mfn2 agonists reverse mitochondrial defects in clinical models of charcot-marie-tooth disease type 2a. *Science* **2018**, *360*, 336–341.
- (16) Dang, X.; Zhang, L.; Franco, A.; Li, J.; Rocha, A. G.; Devanathan, S.; Dolle, R. E.; Bernstein, P. R.; Dorn, G. W., II Discovery of 6-phenylhexanamide derivatives as potent stereoselective mitofusin activators for the treatment of mitochondrial diseases. *J. Med. Chem.* **2020**, *63*, 7033–7051.

- (17) Franco, A.; Dang, X.; Walton, E. K.; Ho, J. N.; Zablocka, B.; Ly, C.; Miller, T. M.; Baloh, R. H.; Shy, M. E.; Yoo, A. S.; Dorn, G. W., II Burst mitofusin activation reverses neuromuscular dysfunction in murine cmt2a. *eLife* **2020**, *9*, No. e61119.
- (18) Yan, L.; Huo, P.; Hale, J. J.; Mills, S. G.; Hajdu, R.; Keohane, C. A.; Rosenbach, M. J.; Milligan, J. A.; Shei, G. J.; Chrebet, G.; Bergstrom, J.; Card, D.; Mandala, S. M. Sar studies of 3-arylpropionic acids as potent and selective agonists of sphingosine-1-phosphate receptor-1 (s1p1) with enhanced pharmacokinetic properties. *Bioorg. Med. Chem. Lett.* **2007**, *17*, 828–831.
- (19) Thorarensen, A.; Wakefield, B. D.; Romero, D. L.; Marotti, K. R.; Sweeney, M. T.; Zurenko, G. E.; Rohrer, D. C.; Han, F.; Bryant, G. L., Jr. Preparation of novel anthranilic acids as antibacterial agents. Extensive evaluation of alternative amide bioisosteres connecting the a- and the b-rings. *Bioorg. Med. Chem. Lett.* **2007**, *17*, 2823–2827.
- (20) Shiozaki, M.; Maeda, K.; Miura, T.; Ogoshi, Y.; Haas, J.; Fryer, A. M.; Laird, E. R.; Littmann, N. M.; Andrews, S. W.; Josey, J. A.; Mimura, T.; Shinozaki, Y.; Yoshiuchi, H.; Inaba, T. Novel n-substituted 2-phenyl-1-sulfonylamino-cyclopropane carboxylates as selective adams-5 (aggrecanase-2) inhibitors. *Bioorg. Med. Chem. Lett.* **2009**, *19*, 1575–1580.
- (21) Talele, T. T. The "cyclopropyl fragment" is a versatile player that frequently appears in preclinical/clinical drug molecules. *J. Med. Chem.* **2016**, *59*, 8712–8756.
- (22) Poduslo, J. F.; Curran, G. L.; Berg, C. T. Macromolecular permeability across the blood-nerve and blood-brain barriers. *Proc. Natl. Acad. Sci. U.S.A.* **1994**, *91*, 5705–5709.
- (23) Reinhold, A. K.; Rittner, H. L. Characteristics of the nerve barrier and the blood dorsal root ganglion barrier in health and disease. *Exp. Neurol.* **2020**, *327*, No. 113244.
- (24) Heiman-Patterson, T. D.; Deitch, J. S.; Blankenhorn, E. P.; Erwin, K. L.; Perreault, M. J.; Alexander, B. K.; Byers, N.; Toman, L.; Alexander, G. M. Background and gender effects on survival in the tgn(sod1-g93a)1gur mouse model of als. *J. Neurol. Sci.* **2005**, *236*, 1–7.
- (25) Guyenet, S. J.; Furrer, S. A.; Damian, V. M.; Baughan, T. D.; La Spada, A. R.; Garden, G. A. A simple composite phenotype scoring system for evaluating mouse models of cerebellar ataxia. *J. Vis. Exp.* **2010**, No. e1787.
- (26) Misko, A.; Jiang, S.; Wegorzewska, I.; Milbrandt, J.; Baloh, R. H. Mitofusin 2 is necessary for transport of axonal mitochondria and interacts with the miro/milton complex. *J. Neurosci.* **2010**, *30*, 4232–4240.
- (27) Kruppa, A. J.; Buss, F. Motor proteins at the mitochondria-cytoskeleton interface. *J. Cell Sci.* **2021**, 134.
- (28) Dorn, G. W., II Mitofusins as mitochondrial anchors and tethers. *J. Mol. Cell. Cardiol.* **2020**, *142*, 146–153.
- (29) Lacivita, E.; Niso, M.; Mastromarino, M.; Garcia Silva, A.; Resch, C.; Zeug, A.; Loza, M. I.; Castro, M.; Ponimaskin, E.; Leopoldo, M. Knowledge-based design of long-chain arylpiperazine derivatives targeting multiple serotonin receptors as potential candidates for treatment of autism spectrum disorder. *ACS Chem. Neurosci.* **2021**, *12*, 1313–1327.
- (30) Idrick, G. M. *SHELXTL-2014, Crystallographic Computing System*; Bruker Analytical X-Ray Instruments: Madison, WI, 2014.
- (31) Sheldrick, G. M. A short history of SHELX. *Acta Crystallogr., Sect. A: Found. Crystallogr.* **2008**, *64*, 112–122.